People's Democratic Republic of Algeria

Ministry of Higher Education and Scientific Research

SAAD DAHLAB Blida-1 University

Faculty of Technology

Department of Renewable Energies

Thesis Presented for the Graduation of the Master's Degree

Specialty: Renewable Energy

Option: Thermal conversion

Theme:

Study of the Influence of the Characteristic's Fin on the Performance of a Collector with Finned Absorber of an Indirect Solar Dryer

Presented by: **Kaddour Amdjed**

Defended before the jury composed by:

F. Ferradji	**MCB**	President
K. Mehalaine	**MCB**	Examiner
R. Bellatreche	**MAA**	Examiner
N.E. Khelalfa	**MCB**	Supervisor
Dr.Kodifa abdelmalek		Co-supervisor

July 2023

ABSTRACT

الملخص

من أجل تعزيز أداء المجفف الشمسي الغير مباشر، من الضروري تحسين ضعف نقل الحرارة بين لوحة الامتصاص والهواء الداخل لمجمع الهواء. تركز هذه الدراسة على تأثير خصائص الزعانف على عملية نقل الحرارة بين الهواء الداخل ولوحة امتصاص الزعانف. من خلال زرع الزعانف على لوحة الامتصاص، من المتوقع تحسين كفاءة نقل الحرارة وبالتالي تعزيز الأداء العام للمجفف الشمسي. يهدف العمل الحالي إلى تحليل تصميمات الزعانف المختلفة وتأثيرها على خصائص نقل الحرارة داخل النظام، عن طريق تغيير سمك الزعنفة (0.001، 0.003، 0.005 متر)، مادة الزعنفة (الفولاذ الخفيف، الألمنيوم والنحاس) وموضع الزعنفة في جامع الهواء من مجفف الطاقة الشمسية الغير مباشر. حيث يكون تدفق الهواء المطبق في الدراسة هو الحمل الحراري الطبيعي. يتم إجراء عمل محاكاة باستخدام برنامج Fluent 6.2 و Fluent 19.2 ، لتقييم الأداء الحراري لتكوينات الزعانف المختلفة ، مما يؤدي إلى رؤى قيمة لتعزيز مجففات الطاقة الشمسية غير المباشرة. في النتائج، وجدنا أن هناك تأثير واضح عند إضافة زعانف متوسط 3 ٪ أعلى من دون زعانف. جامع الهواء بسماكة زعنفة 0.001 أعلى بنسبة 0.299 ٪ و0.799 ٪ تقريبا من سمك الزعنفة 0.003 و0.005 على التوالي. وبالنسبة للموضع الزعنفة هناك تأثير أيضا. ويظهر كل هذا في الفصل الأخير. إذن من هذه الأطروحة نستنتج أن الزعانف ترفع من مساحة التبادل الحراري وتجانس السوائل.

الكلمات المفتاحية:

المجفف الشمسي، الزعانف، مجمع الهواء، لوحة امتصاص بزعنفة.

Abstract

In order to enhance the performance of an indirect solar dryer, it is crucial to improve the poor heat transfer between the absorber plate and the inlet air in the air collector. This study focuses on the impact of fins characteristics on the heat transfer process between the inlet air and the finned absorber plate. By implanting fins onto the absorber plate, it is expected to optimize the heat transfer efficiency and thereby enhance the overall performance of the solar dryer. The present work aims to analyze various fin designs and their influence on the heat transfer characteristics within the system, by change fin thickness (0.001,0.003,0.005 m), fin material (M.S, AL, CU) and fin position in the air collector of indirect solar dryer, Where the air flow applied in the study is the natural convection. A simulation work is conducted by using Fluent 6.2 and 19.2, to evaluate the thermal performance of different fin configurations, leading to valuable insights for the enhancement of indirect solar dryers. In the results, we found that there is a clear effect when adding fins average 3 % higher than without fins. Air collector with 0.001 fin thickness is approximately 0.299% And 0.799% higher than with 0.003 and 0.005 fin thickness respectively. And for the fin position there an effect too. And all of this is shown in the last chapter. So from this thesis we conclude that the fins increase the heat exchange area and the fluid homogeneity.

Key Word:

Solar dryer, fins, Air collector, finned absorber plate.

ACKNOWLEDGMENT

I thank Allah the Almighty, for having given me the courage and the desire to complete my work of recharging. Alhamdulillah.

To my respected teachers;

From the earliest days of elementary school to the challenging years of university, you have been my guiding lights. Your dedication, passion, and commitment to education have inspired me to strive for excellence. I am grateful for your patience, guidance, and unwavering belief in my abilities. You have nurtured my thirst for knowledge and shaped my academic journey in ways I will forever be thankful for.

DEDICATION

To my beloved family;

Thank you for your unwavering love, encouragement, and support. Your belief in my abilities and relentless motivation have been instrumental in my success. Your sacrifices, both big and small, have shaped me into the person I am today. I am blessed to have such a caring and nurturing family by my side, and I will forever cherish the values and lessons you have instilled in me.

To my dear friends;

I am incredibly grateful for the friendship we share. Your presence in my life has brought joy, laughter, and a sense of belonging. Thank you for standing by me during the highs and lows, for being my confidants, and for celebrating my achievements. Your unwavering support and belief in me have been invaluable.

Today, as I complete my dissertation, I am humbled and overwhelmed by the love and support I have received from all of you. Your collective presence in my life has been instrumental in my growth and achievements. I feel truly blessed to have such remarkable individuals by my side, and I am honored to have your continuous support.

With heartfelt gratitude

Kaddour Amdjed

CONTENTS

SYMBOLS

A	area, m^2
Bi	Biot number
C	Specific heat, J/Kg. K
C_P	specific heat at constant pressure, J/Kg. K
$\dot{E}_{in}$	rate of energy transfer into a control volume, W
$\dot{E}_{out}$	rate of energy transfer out of control volume, W
Gr	Grashof number
L	characteristic length, m
M	mass, Kg
Nu	Nusselt number
P	Perimeter, m
Pr	Prandtl number
Ra	Rayleigh number
T	temperature, K
V	volume, $m^{3;}$ fluid velocity, m/s
g	gravitational acceleration, m/s^2
h	convection heat transfer coefficient, W/m^2. K
h_r	radiation heat transfer coefficient, W/m^2. K
k_a	Thermal conductivity of air, W/m^2. k
q	heat transfer rate, W
t	time, s

Greek Letters

α	Absorptivity; thermal diffusivity, m^2/s
β	volumetric thermal expansion coefficient, K^{-1}
θ	temperature difference, K
μ	viscosity, Kg/s.m
v	kinematic viscosity, m^2/s
ρ	mass density, Kg/m^3
σ	Stefan-boltzmann constant (5.68×10^{-8}) W/m^2. K^4
τ	transmittance

Subscripts

am	ambient conditions
abs	absorber plate
cd	conduction
M.S	Mild steel
sky	sky conditions
x	local conditions on a surface
∞	free stream conditions

LIST OF FIGURES

LIST OF TABLES

General Introduction:

The world is suffering from pollution and harmful greenhouse gases originated from burning of fossil fuels where the consequences of climate changes are also alarming. Solar energy is an alternative energy source that is abundant, safer and cleaner.

Algeria disposes of an important potential of renewable energies, such as geothermal, biomass, solar and wind energy. However, referring to the guide published by the Algerian Ministry of Energy and Mining, in 2007 [1], solar energy plays the most important role. Effectively, and following the same source and the World Energy Council report, the insolation duration in Algeria is around 2650 h per year for the coastal regions, 3000 h per year for the high plateau regions and it increases to 3500 h per year for the Sahara. [1]

Solar drying is one of the processes that have found application in Algeria, because of the important quantities of solar irradiations that can be exploited in this country. Nevertheless, the experience of Algeria in solar drying is recent and limited to drying of fruits, vegetables, medicinal and aromatic herbs. [1]

Exploiting solar energy for the drying process is very should be developed in Algeria because of their great solar energy potential. Algeria is a country that only has 2 ‘big’ seasons and the sun shines for 12 hours a day.

One of the efforts to improve the performance of solar dryers is to use fins. The use of fins serves to increase the area of heat absorption without increasing the dimensions of the solar dryers [2]. Research is attempting study the effect of different types of fins to optimize the performance of solar dryer type.

In order to enhance the performance of the indirect solar dryer, and solving the problem of poor heat transfer between the absorption plate and the incoming air in the air collector. This study focuses on the influence of fine properties on the heat transfer process between the incoming air and the fin absorption plate. By implanting the fins on the absorption plate, it is expected to improve the heat transfer efficiency and thereby enhance the overall performance of the solar dryer. The current work is aimed at analyzing various fin designs (dimensions, material, disposition.) and their influence on the heat transfer properties inside the indirect solar dryer where the air flow applied in the study is the natural convection.

In the first chapter we made a general presentation on the solar drying operation and major properties.

The theoretical analysis study and the different heat balances presented for the air collector of the indirect solar dryer in the second chapter.

The modeling and CFD analysis and the simulation working method, boundary condition, geometries, meshing, are presented in the second chapter.

In the last chapter, we draw the results obtained from the simulation in the form of curves, and discuss them with the conclusion for each case. The thesis is closed with a general conclusion compromised all the points taken from the chapters.

CHAPTER I

BIOGRAPHICAL STUDY

Introduction:

Drying is a process that has been used by humans for thousands of years to preserve food, clothing, and other materials. In solar dryer, solar energy is used as either the sole sources of the required heat or as supplemental sources. The air flow can be generated by either natural (passive mode) or forced convection (active mode). The heating procedure could involve the passage of preheated air through the product or by directly exposing the product to solar radiation or a combination of both.

I.1 Passive and Active Mode:

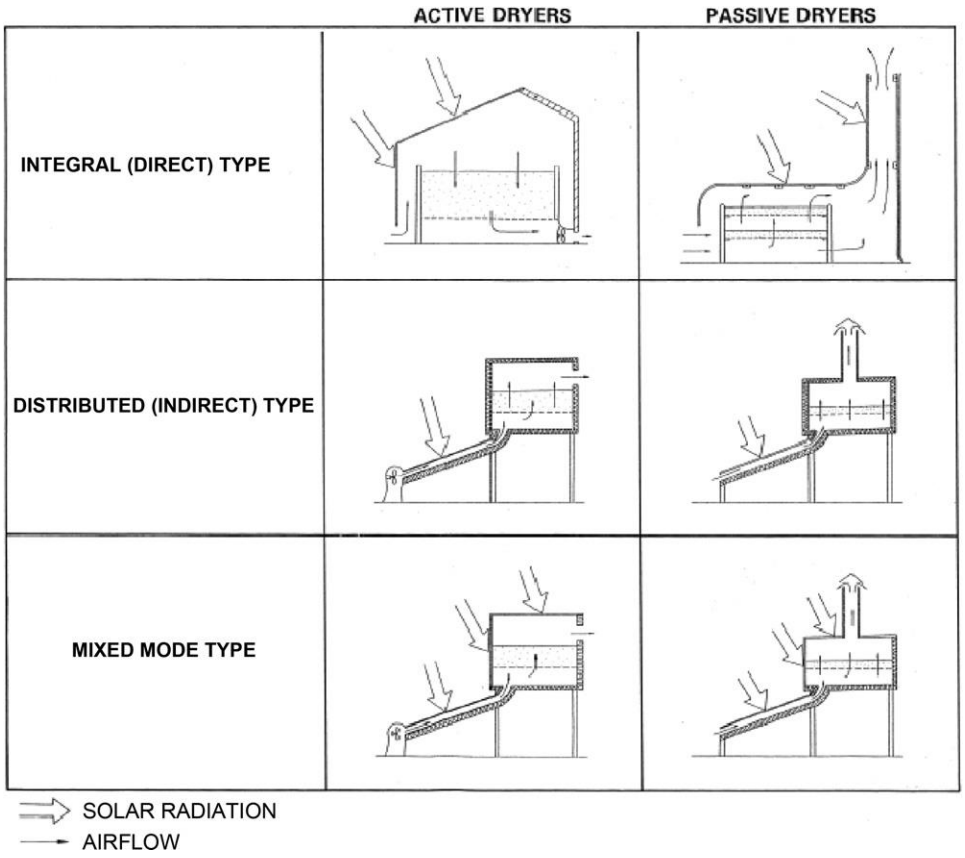

Figure I.1 Presentation of the different functioning modes and types of solar dryers [1]

- **Passive mode:** Passive solar dryers are often referred to as natural ventilation solar dryers, where no external source of energy is required to run the dryer. In this dryer, incoming air is heated up with the help of solar energy. The hot air then passes over the crop's surface. The thermosiphon effect combined with the greenhouse effect is the main operators for natural ventilation.

- **Active mode:** After open sun drying, passive solar dryer came into use and then an active solar dryer was developed, working on the principle of the forced convection mode of heat transfer. Fans or a blower are used to increase the airflow rate so that enhanced heat transfer takes place.

I.2 Basic Types of Solar Dryers:

I.2.1 Direct Type Dryers:

Direct type dryers are like a cabinet with a compartment with a glass roof. Here solar rays directly fall onto the commodity through the glass and with the greenhouse effect, it's been heated. The airflow carries away the moisture as shown below. Tunnel, Greenhouse, and cabinet-type dryers fall into this category.

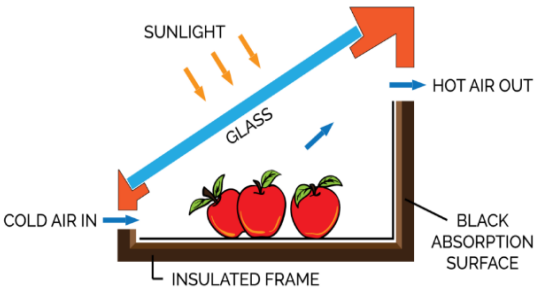

Direct (a)

Cabinet (b)

Greenhouse (c)

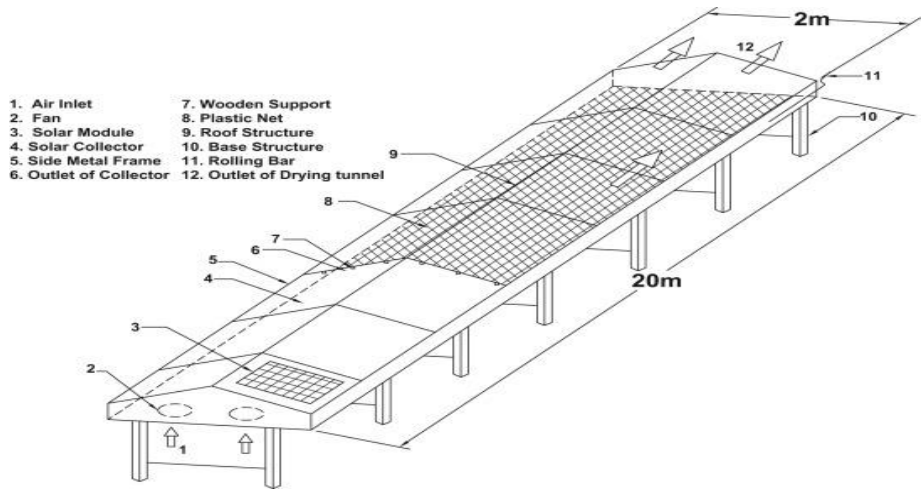

Triangular Roof Tunnel (d)

Figure I.2 (a),(b),(c)and (d) Schematic of Direct Solar Dryer and Examples [3]

I.2.2 Indirect Type Dryers:

Indirect type solar dryers have separate chambers for drying and heating airflow. In this case, there's no direct contact between solar rays and commodity as shown in the figure below. Airflow entering from solar collector gets heated up and carries away the moisture from drying chamber.

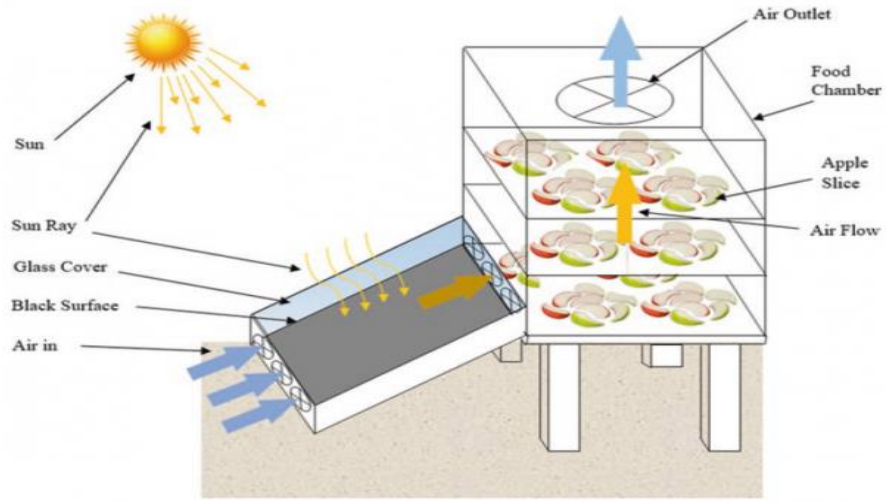

Figure I.3 Schematic of Indirect Solar Dryer [3]

I.2.3 Mixed-Mode Dryers:

Mixed-mode dryers are a combination of above two types. The structure is similar to indirect dryer but drying chamber is made of transparent material so that the solar collector and drying chamber both get heated up by the greenhouse effect.

Figure 1.4 Schematic of mixed solar Dryer [3]

I.3 The Drying Process:

It is divided on three steps

- Converting Light into Heat: the presence of black inside a solar dryer improves the efficiency of the transformation of light into heat.

- Trapping Heat: insulating the air inside the dryer from the outside air makes a significant difference. Using a transparent solid, such as a plastic bag or glass lid, allows light to enter, but once the light is absorbed and converted to heat, the plastic bag or glass lid traps the heat inside to dehydrate the food. This makes it possible to achieve similar temperatures in cold, windy weather as in hot weather.

- Move Heat to the Food: Both the natural convection dryer and the forced convection dryer use heated air convection to move heat to the food. When the heated air enters to the hot chamber, the humidity in the air decreases, allowing dehumidification and drying of fruits for example.

I.4 Advantages of solar drying:

- The rate of drying increases with higher temperature and movement of air in the chamber.
- Food is enclosed in the dryer and therefore protected from dust, insects, birds, and animals.
- Higher temperature prevents insect infestation and the faster drying rate reduces the risk of spoilage by microorganisms.
- The dryers are waterproof, therefore, the food does not need to be moved during the rainy season.
- A dryer can be constructed from locally available materials at a relatively low cost.
- Solar dryers last longer. A typical dryer can last 15-20 years and will need minimum maintenance.

I.5 Limitations with solar drying:

- Can be only used during day time when an adequate amount of solar energy is present.
- Lack of skilled personnel for operation and maintenance.
- Takes longer as compared to the modern type of electric dryers.
- A backup heating system is necessary for products requiring continuous drying.

For these reasons, in order to raise and reduce these limits, many researches and works have been conducted, and some of them are mentioned on the following.

I.6 State of the art:

I.6.1 In Algeria:

In 2002, Miri et al. [4] have developed an indirect solar dryer working on natural convection. The chart of this solar dryer is illustrated in **Figure I.5**. It is constituted of two essential parts: the solar collector and the drying chamber. The solar collector is heating air with double circulation; the first between the glass cover and absorber and the second between the absorber and the bottom part. This last part and the lateral walls are thermally isolated. The results obtained by the collector with double circulation were compared with one with simple circulation. Hence, the temperature of the absorber of simple circulation has attained 103.31 °C and was 96.55 °C for double circulation. The most important temperature to be known is one of the heated air that goes to the drying chamber. It was around 60 °C, for a simple circulation collector and around 50 °C for a double circulation. The calculated efficiency of the solar dryer was around 40% which was an encouraged result.

Figure I.5 Natural convection solar dryer – indirect type developed in D.C.R.E. [4]

In 2002, a comparison between the direct natural solar cabinet dryer and the indirect natural one was made by Benkhelfellah et al. [5] The results were relatively favorable to the direct solar cabinet dryer, as we register 70% of extracted pepper humidity in 72 h against 243 h for the indirect dryer. Also drying grapes needed 268 h using direct dryer against 318 h for the indirect solar dryer. But 67% of the humidity of vervain was extracted in 48 h using direct natural solar dryer and it was only 30 h for extracting 75% of its humidity using the indirect natural solar dryer.

In 2007, Benaouda and Belhamel [6] and in 2008, Boulemtafes-Boukadoum et al. [7] have developed a solar dryer shown in **Figure I.6**. As well this dryer is constituted of 2 main parts; the solar collector and the drying chamber. The solar collector is a simple one with simple air circulation, its dimensions were: 2m ×0.94m, built with galvanized sheet-iron. The same matter painted in black (in order to increase the absorption properties) is used as absorber. It has a 0.0005m thick and the value of its thermal conductivity was 54Wm^{-2} K. The collector is covered with a 0.003m thick of

ordinary glass. The use of a thermos regulator tool allows performing drying with air heated to a constant 50 °C. Several products were tested such as tomatoes, tobacco, figs, mint and laurel and depending on the product; the drying time varies from 5 to 10 h. The dryer has given satisfactory results; however, the quantities were not important.

Figure I.6 Indirect forced convection dryer developed in D.C.R.E [6, 7]

In 2017, Messaoud Sandali et al. [8] by numerical simulation (fluent), they study the thermal performance of a direct solar dryer with integration of geothermal water heat exchanger shown in **Figure I.7**. For supply the solar dryer by heat after sunset. The climatic data used in this work were measured in Ouargla city. The temperature of geothermal water in this region was found to be 343K.The smallest obtained value of drying air temperature was found 327K (At night), while the highest obtained value was found 344K(13:00PM).

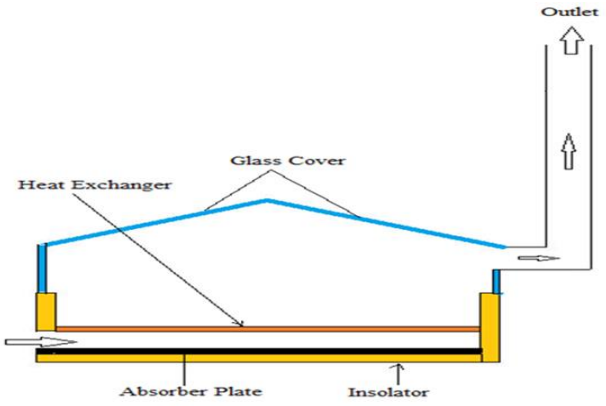

Figure I.7 Direct Solar Dryer with Geothermal Heat Exchanger [8]

For improve the thermal performance of a direct solar dryer, in 2019, Messaoud Sandali et al. [9] They presented a work concerns an experimental study to improve the thermal performance of a direct solar dryer with integration of geothermal water heat exchanger properly tested in the arid North-Saharan regions of Algeria shown in **Figure I.8**. The results in this study showed a significant improvement of the thermal performance of the direct solar dryer, especially after sunset, the smallest obtained experimental value of drying air temperature was found 46 °C, while the highest one was 58 °C. After sunset and throughout all the night until the sunrise, the drying air temperature remains important and almost steady with an average value of 46 °C and exceeds that in case of solar dryer without heat exchanger by 30° C.

Figure I.8 Direct Solar Dryer with Heat Exchanger [9]

I.6.2 Other Countries:

In 2010, B.M.A. Amer et al. [10] study a hybrid solar dryer, which consists of solar collector, reflector, heat exchanger cum heat storage unit and drying chamber shown in **Figure I.9**. The drying chamber was located under the collector. The dryer was operated during normal sunny days as a solar dryer, and during cloudy day as a hybrid solar dryer. Drying was also carried out at night with stored heat energy in water which was collected during the time of sunshine and with electric heaters located at water tank. The efficiency of the solar dryer was raised by recycling about 65% of the drying air in the solar dryer and exhausting a small amount of it outside the dryer.

In 2016, S. Nabnean et al. [11] by an experimental work, a new design of a solar dryer shown in **Figure I.10**, which consists of drying cabinet, heat exchanger, 16-m^2 water type solar collector, and water type heat storage unit. The cabinet size is 1.0 m wide 3.0 m long 1.4 m high with the load capacity of 100 kg for drying osmotically dehydrated cherry tomatoes. In the results the Drying air temperature was varied between 30 °C and 65 °C during drying.

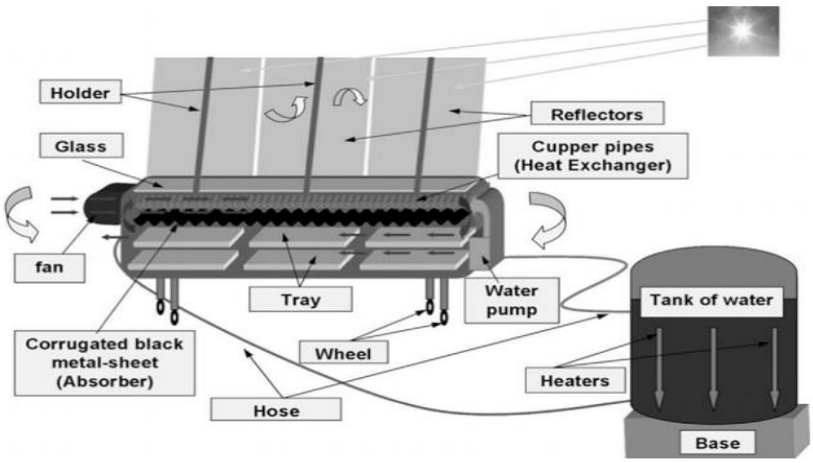

Figure I.9 Schematic Diagram of a Hybrid Solar Dryer [10]

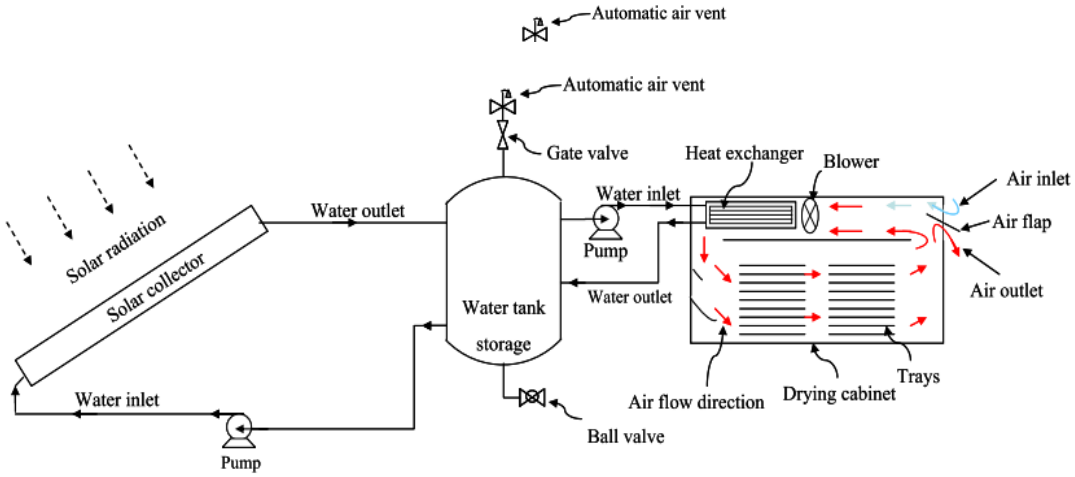

Figure I.10 Schematic Diagram of a Solar Dryer [11]

In 2017, M. Yahya et al. [12] investigated a hybrid solar-biomass dryer for drying paddy shown in **Figure I.11**. In this system, the air from surrounding entered into the solar collector and received some heat before it travelled to the biomass furnace. The air was further heated up in the biomass furnace and subsequently moved to the fluidized bed where the paddy was placed. The investigated drying system was able to reduce the moisture content of paddy from 20% to 6%, with average drying temperature of 61°C and 78°C.The average thermal efficiency and exergy efficiency were 13.45% and 47.6% respectively for drying temperature of 61°C. For drying temperature of 78°C, the system was able to achieve average thermal efficiency of 16.28% and exergy efficiency of 49.5%.

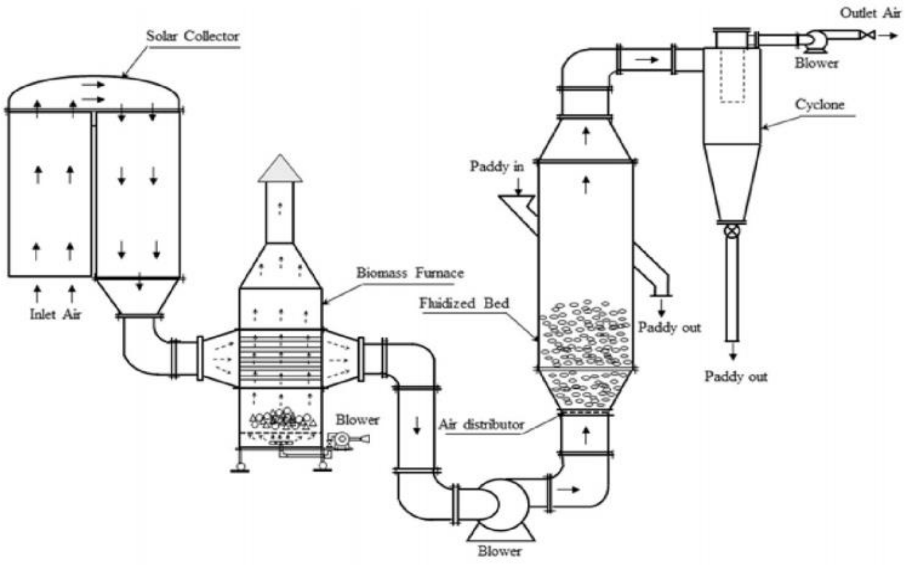

Figure I.11 Schematic Diagram of a Solar-Biomass Dryer [12]

In 2017, T. Bhattacharyyaa et al. [13] study a Finned Plate air heating solar collector for paddy drying shown in **Figure I.12**, with rectangular fins attached is studied theoretically for various controlling parameters such as numbers of fins, H/D ratios and fin thicknesses to use it for paddy drying. Outlet air temperature first increases and then decreases with number of fins. Pressure drop also increases with number of fins and fin height. To choose the optimum number and height of the fins both the outlet air temperature and pressure drop are taken into consideration and the design with 80 numbers of fins and 0.6 H/D ratio with 2 mm fin thickness is chosen to be optimum. The optimum design of solar air heater produces higher outlet temperature at steady state than required.

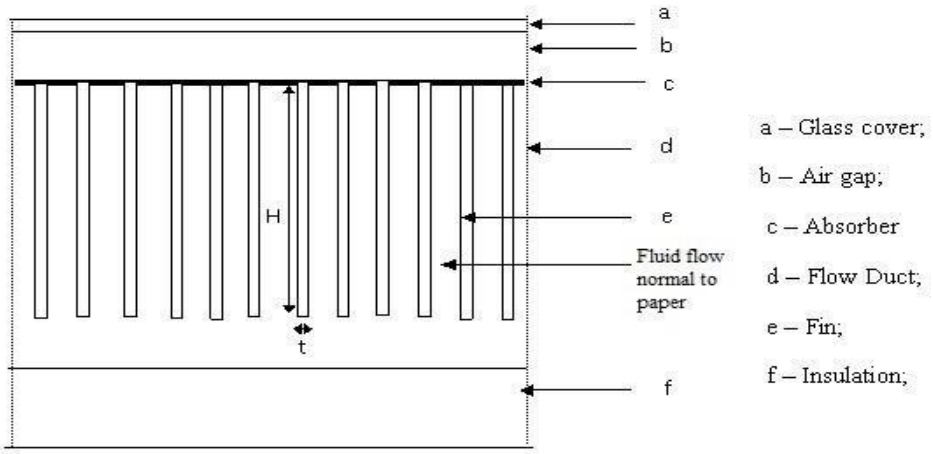

Figure I.12 Schematic diagram of finned plate solar air heater [13]

In 2018, Panuwat Pawakote and Atit Koonsrisuk. [14] investigated the performances of a solar collector with fins and baffles numerically and experimentally shown in **Figure I.13**. It was found that the experimental efficiency and outlet temperature are about 47.27% and 60.1°C, respectively. While the predicted efficiency and outlet temperature is about 52.01% and 64.9°C, respectively. The discrepancy could be due to heat losses from the walls of the air passages.

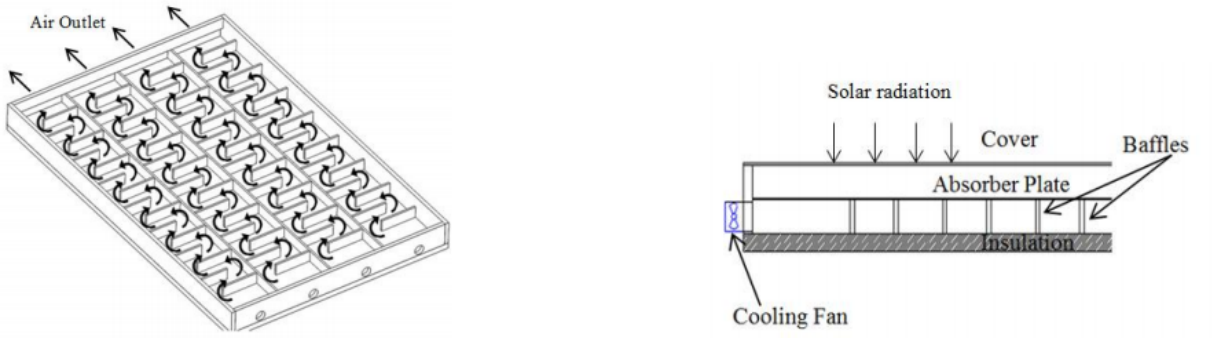

Figure I.13 Schematic diagram of Solar Collector with Fins and Baffles [14]

In 2018, The work of C. UMA MAHESWARI1et al. [15] shown in **Figure I.14** focuses on numerical analysis using CFD CFX 14.0 and experimental analysis of the solar crop dryer attached with flat plate collector and the waste heat recovery of exhaust gas from the diesel engines used in the agricultural fields for water pumping. A comparison study was made between the crop dryer with and without exhaust pipe heat exchanger (with and without fins) and found that when the exhaust pipe was attached there was an improvement in the increase in temperature compared without exhaust pipe. The copper tubes of exhaust pipe were also added with the fins to improve its heat exchanging efficiency.

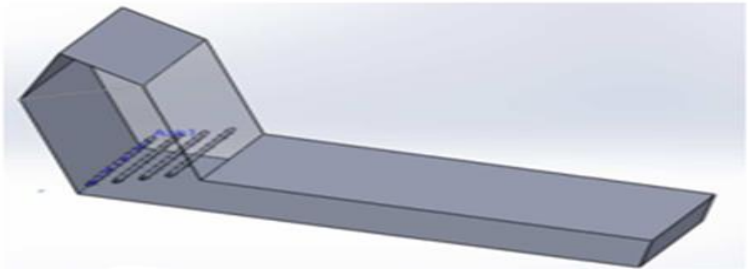

Figure I.14 Food Dryer with an Exhaust Tube and Copper Fins [15]

In 2020, Satyapal Yadav and V.P. Chandramohan. [16] made A 2D numerical study to identify the effect of fins on thermal energy storage (TES) device of indirect type solar dryer (ITSD) shown in **Figure I.15**. Two models have been developed to study the above behavior, one being TES device without fins (case – I) and the second one with fins (case – II). CFD simulations were carried out for four air velocity conditions and a comparative study was performed in both cases. It was found that both cases work fine with an air velocity of 1 m/s compared to higher air flow velocities (2 to 4 m/s).and the Maximum heat gained by the air for case – II is 55.2% more compared to case – I at an air velocity of 1 m/s.

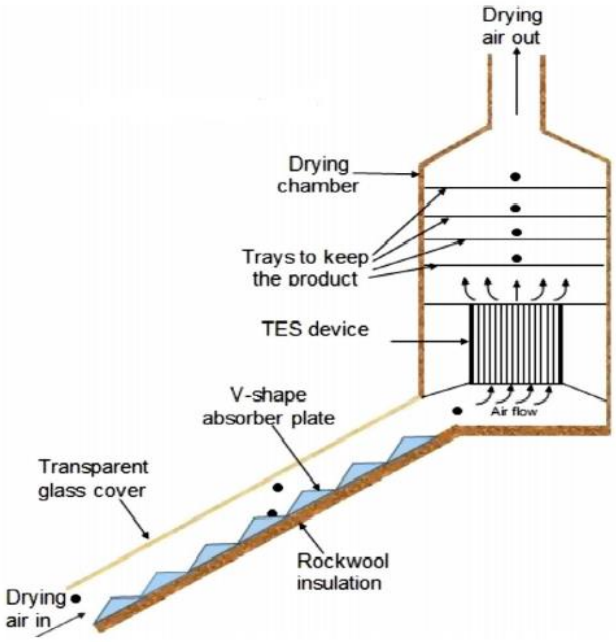

Figure I.15 Schematic of indirect type solar dryer (ITSD) setup with sensors location [16]

In 2020, S. Murali et al. [17] presented an experimental work. The study was aimed at design and development of an energy efficient solar dryer suitable for continuous drying operation. In this dryer, water was used as a thermal energy storage and heat transfer medium, and air as an intermediate fluid. The major parts of the dryer were flat-plate solar water collector, water storage tank, drying chamber, heat exchanger, and liquefied petroleum gas (LPG) water heater shown in **Figure I.16**. The dryer was designed to work mostly on solar energy during peak sunshine hours and LPG water heater as auxiliary heat source during low sunshine hours. The maximum collector outlet temperature of 73.5°C. Overall, solar system supplied 73.93% of heat energy and LPG water heater assisted rest of the energy requirement due to lower incident solar radiation during start and end of drying. The maximum collector and drying efficiency obtained for shrimp drying were 42.37% and 37.09%, respectively.

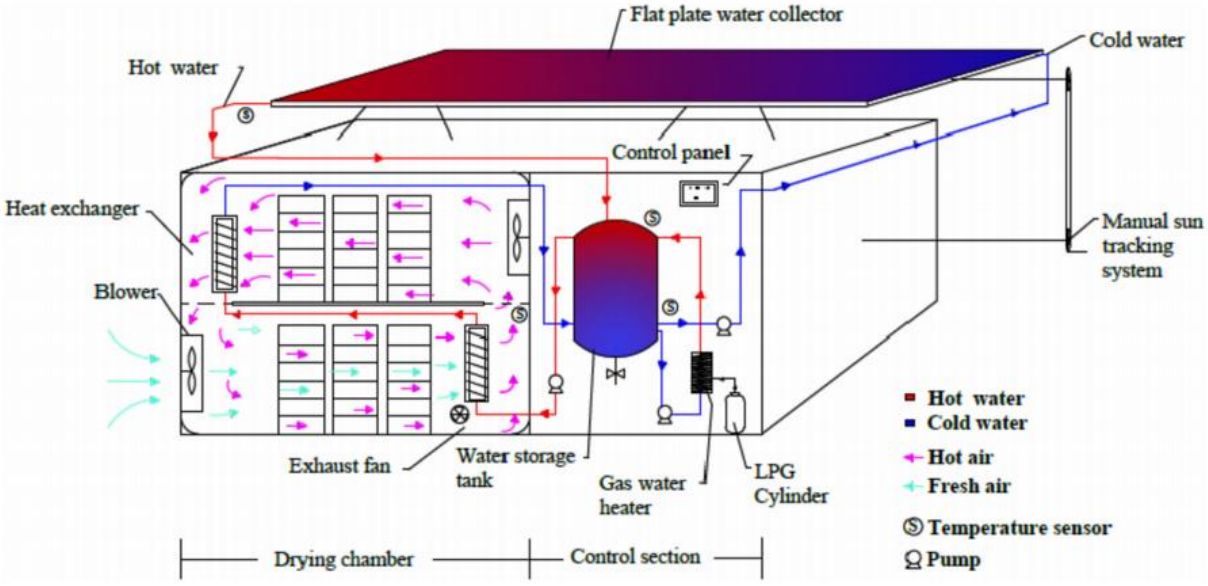

Figure I.16 Schematic diagram of Solar-LPG Hybrid Dryer [17]

In 2021, Cristiana Brasil Maia et al. [18] by an experimental study they presented a hybrid solar dryer with baffles disposed of on the solar collector shown in **Figure I.17**. When the levels of solar radiation are low, an electrical heater is used to increase the drying air temperature. A photovoltaic system feeds the electrical heater and the fans. The Results indicated that the baffles augmented the energy efficiency of the system (from 23.5 to24.9%).

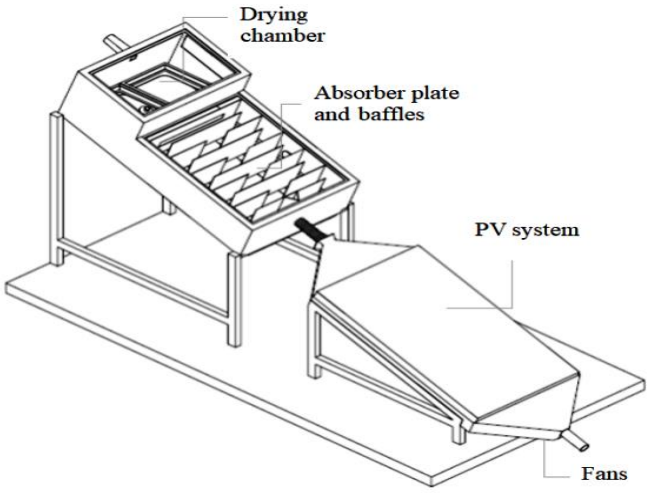

Figure I.17 Schematic of the Dryer [18]

In 2021, Erdem Çiftçi et al. [19] study, two vertical PVT dryers with and without fins shown in **Figure I.18**, by a numerical and experimental work. Fins have been integrated over absorber and PV surface to increase heat transfer and regulate air flow. Both numerical simulation results and experimental findings clearly illustrated the positive effects of fins. In the experiments conducted at 0.010, 0.012 and 0.014 kg/s flow rate in the PVT without fins, average thermal efficiency values were achieved as 47.46%, 52.36% and 54.86%, respectively. In addition, in the performance tests done at 0.010, 0.012 and 0.014 kg/s mass flow rate in the PVT with fins, average efficiency values were attained as 50.25%, 55.83% and 58.16%, respectively.

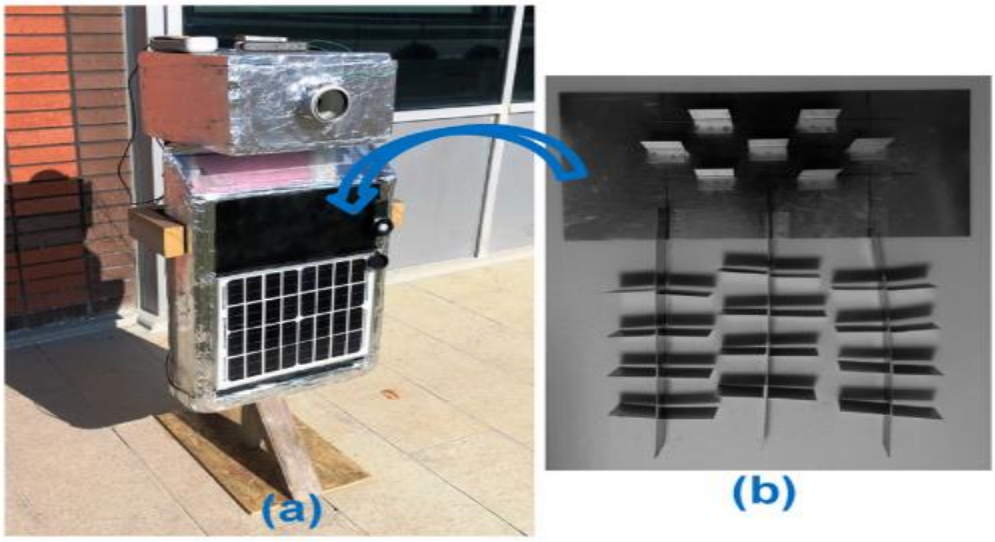

Figure I.18 A photograph of experimental setup (a) and designed fin geometry (b) [19]

In 2023, S. Madhankumar et al. [20] in an experimental study shown in **Figure I.19**, three different corrugated absorber plate solar collector setups (without Phase Change Material Energy Storage (PCMES), with PCMES, and with fins inserted PCMES) for a solar dryer. The ISD with fins inserted PCMES performed better than the other two setups in energy performances. However, because of the usage of fins, the same setup has a slightly higher (3.1%) capital cost than the setup without fins. ISD with fins inserted PCMES is chosen as the best setup based on energy and economic parameters from the multiple criteria decision-making techniques.

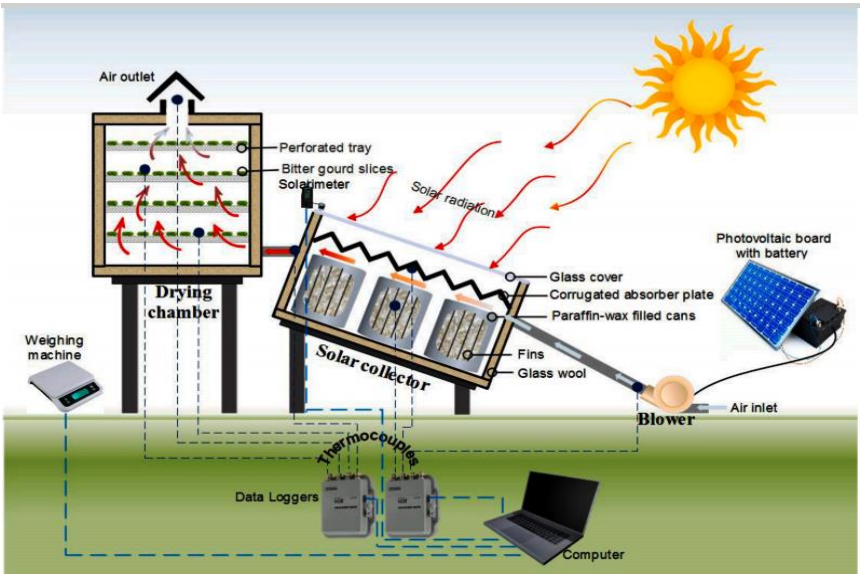

Figure I.19 Schematic representation of the ISD with instruments [20]

I.7 General Information of Different Dryers:

Different types of dryers have their unique advantages. There's no 'best' option for all applications. Taking into the nature of the commodity and other factors, best fit can be chosen. Therefore, it is better to know some facts and figures of different drying mechanisms shown in **Table I.1.**

Table I.1 General Information for Different Dryers [1]

	Direct Solar Dryer	**Indirect Solar Dryer**
	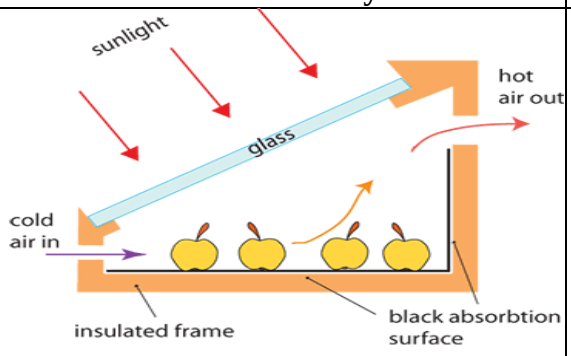	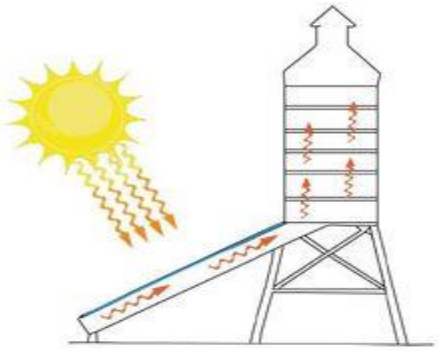
Operating Temperature	Medium T usage (45-78 ˚C)	Medium T (45-75 ˚C)
Scale of Operation	Applicable in small to industrial scale	Better in small scale usage
Need of Solar Collector	No solar collector	Solar collector must
Type of Commodity	Can also be used for products where direct solar contact is mandatory	Can also be used for products where direct solar contact is not mandatory
Performance in unfavorable weather	Operatable even in unfavorable weather	Poor performance in unfavorable weather

I.8 Factors that Affecting the Efficiency of the Solar Dryer:

I.8.1 Physical Characteristics of the Dryer:

- Type, size, shape and drying capacity.
- Surface of the drawers and their number.
- Modality of loading and unloading.

I.8.2 Thermal Performance:

- Drying time and air flow.
- Dryer air temperature, solar irradiation and relative humidity.

I.8.3 Dried Product Quality:

- The product that we going to during it.

Conclusion:

Overall, all these dryers can be made with locally available materials and still can achieve better quality products than open sun-dried products. But, understanding the nature of the product, applying proper materials, selecting appropriate mechanisms, and controlling the optimum conditions will make your dryer more productive and sustainable while making better profit margins.

CHAPTER II

THEORETICAL ANALYSIS

Introduction:

This work focuses on the indirect dryer in general and the solar collector in particular. The role of a thermal solar collector is to transform the solar radiation it receives, into usable calorific energy, most often via a heat transfer fluid (water, air…). The basic diagram of a flat solar collector is given in the figure below:

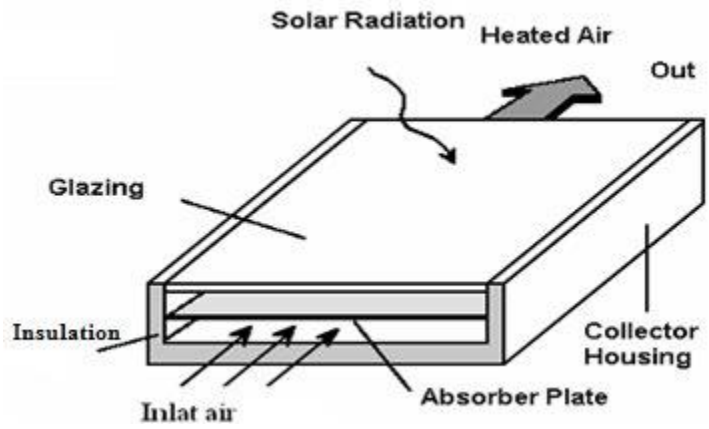

Figure II.1 Principle Diagram of a Flat Air Solar Collector [21]

II.1 Heat Balance Equations for Air Collector:

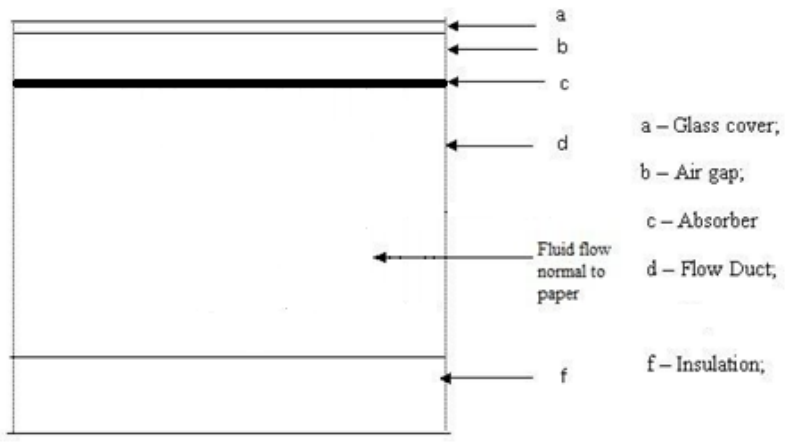

Figure II.2 Schematic diagram of solar air heater [22]

- Glass Cover: (node ‘c ‘)

$$h_{c\text{-}am}(T_{am}-T_c) + h_{r1}(T_{sky}-T_c) + h_{c\text{-}a}(T_a-T_c) + h_{r2}(T_{abs}-T_c) + I\,\alpha_c = M_c\,C_c\frac{dT_c}{dt} \qquad \text{(II.1)}$$

- Air gap: (node ‘a ‘)

$$h_{a\text{-}c}(T_c-T_a) + h_{a\text{-}ab}(T_{ab}-T_a) = M_a\,C_a\frac{dT_a}{dt} \qquad \text{(II.2)}$$

- Absorber: (node ‘abs’)

$$h_{abs\text{-}a}(T_a - T_{abs}) + h_{r2}(T_c - T_{abs}) + h_{abs\text{-}f}(T_f - T_{abs}) + I\,\alpha_{abs}\,\tau_c = M_{abs}\,C_{abs}\frac{dT_{abs}}{dt} \quad \text{(II.3)}$$

- fluid: (node ‘f ‘)

$$h_{f\text{-}abs}(T_{abs} - T_f) + h_{f\text{-}ins\ top}(T_{ins\ top} - T_f) + m_{flow}\,C_f\,(T_{f\text{-}in} - T_{f\text{-}out}) = M_f\,C_f\frac{dT_f}{dt} \quad \text{(II.4)}$$

- Insulation top: (node ‘ins top ‘)

$$h_{ins\ top\text{-}f}(T_f - T_{ins\ top}) + hcd_{ins\ top\text{-}ins\ bot}(T_{ins\ bot} - T_{ins\ top}) = M_{ins\ top}\,C_{ins\ top}\frac{dT_{ins\ top}}{dt} \quad \text{(II.5)}$$

- Insulation bottom: (node ‘ins bot ‘)

$$hcd_{ins\ bot\text{-}ins\ top}(T_{ins\ top} - T_{ins\ bot}) + h_{ins\ bot\text{-}amb}(T_{amb} - T_{ins\ bot}) = M_{ins\ bot}\,C_{ins\ bot}\frac{dT_{ins\ bot}}{dt} \quad \text{(II.6)}$$

II.2 Heat Balance Equations for Air Collector with Fins:

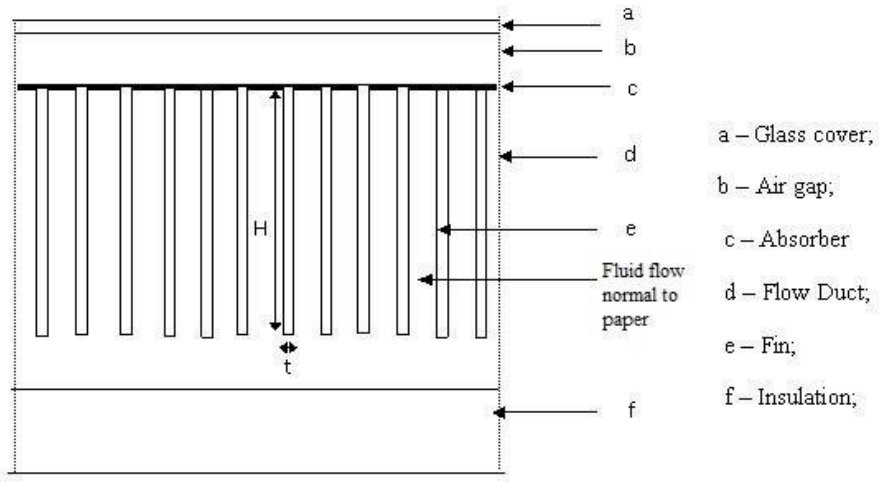

Figure II.3 Schematic diagram of Finned plate solar air heater [22]

- Glass Cover: (node ‘c ‘)

$$h_{c\text{-}am}(T_{am} - T_c) + h_{r1}(T_{sky} - T_c) + h_{c\text{-}a}(T_a - T_c) + h_{r2}(T_{abs} - T_c) + I\,\alpha_c = M_c\,C_c\frac{dT_c}{dt} \quad \text{(II.7)}$$

- Air gap: (node ‘a ‘)

$$h_{a\text{-}c}(T_c - T_a) + h_{a\text{-}ab}(T_{ab} - T_a) = M_a\,C_a\frac{dT_a}{dt} \quad \text{(II.8)}$$

- Absorber: (node ‘abs’)

$$h_{abs\text{-}a}(T_a - T_{abs}) + h_{r2}(T_c - T_{abs}) + h_{cd}(T_{finbase} - T_{abs}) + h_{abs\text{-}f}(T_f - T_{abs}) + I\,\alpha_{abs}\,\tau_c = M_{abs}\,C_{abs}\frac{dT_{abs}}{dt} \quad \text{(II.9)}$$

- Fin base: (node ‘finbase ‘)

$$h_{cd}(T_{abs}-T_{finbase})+h_{cd}(T_{finbase+1}-T_{finbase})+h_{fin\text{-}f}(T_f-T_{finbase})=M_{finbase}C_{finbase}\frac{dT_{finbase}}{dt} \quad \text{(II.10)}$$

- Along the fin: (node ‘fi(n) ‘)

$$h_{cd}(T_{fi(n-1)}-T_{fi(n)})+h_{cd}(T_{fi(n+1)}-T_{fi(n)})+h_{fi(n)\text{-}f}(T_f-T_{fi(n)})=M_{fi(n)}C_{fi(n)}\frac{dT_{fi(n)}}{dt} \quad \text{(II.11)}$$

- Fin tip: (node ‘fintip ‘)

$$h_{cd}(T_{fi(n-1)}-T_{fintip})+h_{fintip\text{-}f}(T_f-T_{fintip})=M_{fintip}C_{fintip}\frac{dT_{fintip}}{dt} \quad \text{(II.12)}$$

- fluid: (node ‘f ‘)

$$h_{f\text{-}abs}(T_{abs}-T_f)+h_{f\text{-}finbase}(T_{finbase}-T_f)+h_{f\text{-}fi(n)}(T_{fi(n)}-T_f)+h_{f\text{-}fintip}(T_{fintip}-T_f)+h_{f\text{-}ins\ top}(T_{ins\ top}-T_f)+m_{flow}C_f(T_{f\text{-}in}-T_{f\text{-}out})=M_fC_f\frac{dT_f}{dt} \quad \text{(II.13)}$$

- Insulation top: (node ‘ins top ‘)

$$h_{ins\ top\text{-}f}(T_f-T_{ins\ top})+hcd_{ins\ top\text{-}ins\ bot}(T_{ins\ bot}-T_{ins\ top})=M_{ins\ top}C_{ins\ top}\frac{dT_{ins\ top}}{dt} \quad \text{(II.14)}$$

- Insulation bottom: (node ‘ins bot ‘)

$$hcd_{ins\ bot\text{-}ins\ top}(T_{ins\ top}-T_{ins\ bot})+h_{ins\ bot\text{-}amb}(T_{amb}-T_{ins\ bot})=M_{ins\ bot}C_{ins\ bot}\frac{dT_{ins\ bot}}{dt} \quad \text{(II.15)}$$

The convective heat loss coefficient from cover to ambient air is given and V is the wind speed over collector in m/s: [23]

$$h_{c\text{-}am}=2.8+3V \quad \text{(II.16)}$$

The radiation heat transfer coefficient is calculated by, [22]

$$h_{r1}=\sigma\varepsilon\frac{(T_c^4-T_{sky}^4)}{T_c-T_{am}} \quad \text{(II.17)}$$

The heat transfer coefficient for radiation between the absorber plate and glass cover is, [22]

$$h_{r2}=\sigma\frac{(T_{abs}^2+T_c^2)(T_{abs}-T_c)}{\frac{1}{\varepsilon_c}+\frac{1}{\varepsilon_{ab}}-1} \quad \text{(II.19)}$$

And for the rest, convective heat transfer coefficients between a plate and fluid is, [22]

$$h=(k_f*Nu)/L \quad \text{(II.20)}$$

II.3 Heat Balance Equations for Fins: [24]

To determine the heat transfer rate associated with a fin, we must first obtain the temperature distribution along the fin. by performing an energy balance on an appropriate differential element. Consider the extended surface of Figure II.4.

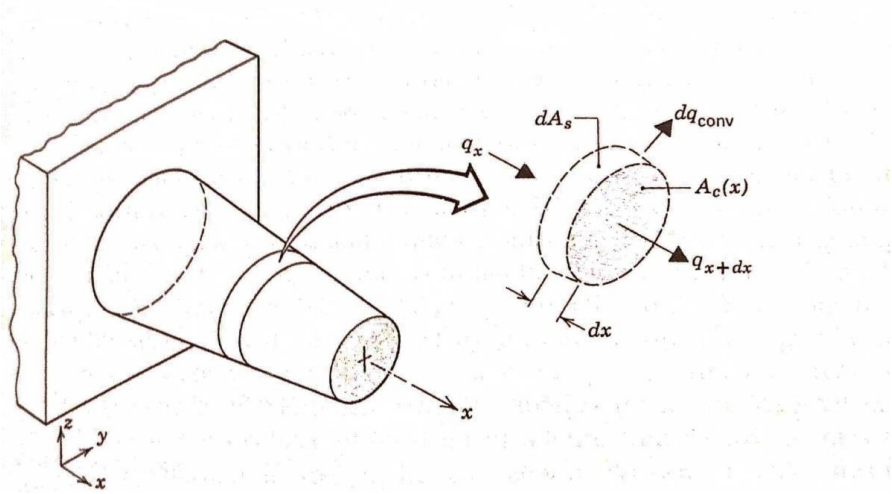

Figure II.4 Energy balance for an extended surface [24]

The analysis is simplified if certain assumptions are made. After the conduction is assumed to be one-dimensional in the longitudinal (x) direction, although the conduction within the fin is in fact two-dimensional. The rate at which energy is convected to the fluid from any point on the fin surface must be balanced by the rate at which energy reaches that point due to conduction in the transverse (y, z) direction. However, in practice the fin is thin and temperature changes in the longitudinal direction are much larger than those in the transverse direction. Hence we may assume one dimensional conduction in the x direction. We will consider steady-state conditions and also assume that the thermal conductivity is constant, that radiation from the surface is negligible, that heat generation effects are absent, and that the convection heat transfer coefficient h is uniform over the surface. Applying the conservation of energy requirement to the differential element of Figure II.4, we obtain [24]

$$q_x = q_{x+dx} + dq_{conv} \tag{II.21}$$

From Fourier's law we know that

$$q_x = - k A_c \frac{dT}{dx} \tag{II.22}$$

Where A_c, is the cross-sectional area, which may vary with x. Since the conduction heat rate at x + dx, may be expressed as

$$q_{x+dx} = q_x + \frac{dqx}{dx} dx \tag{II.23}$$

It follows that

$$q_{x+dx} = - k A_c \frac{dT}{dx} - k \frac{d}{dx}(A_c \frac{dT}{dx}) dx \tag{II.24}$$

The convection heat transfer rate may be expressed as

$$dq_{conv} = h\, dA_s\,(T-T_\infty) \qquad \text{(II.25)}$$

Where dA_s, is the surface area of the differential element. Substituting the foregoing rate equations into the energy balance, Equation II.21, we obtain:

$$\frac{d}{dx}\left(A_c\frac{dT}{dx}\right) - \frac{h}{k}\frac{dAs}{dx}(T-T_\infty) = 0 \qquad \text{(II.26)}$$

Or

$$\frac{d^2T}{dx^2} + \left(\frac{1}{A_c}\frac{dA_c}{dx}\right)\frac{dT}{dx} - \left(\frac{1}{A_c}\frac{h}{k}\frac{dA_s}{dx}\right)(T-T_\infty) = 0 \qquad \text{(II.27)}$$

This result provides a general form of the energy equation for one-dimensional conditions in an extended surface.

II.3.1 Fins of Uniform Cross-Sectional Area Ac: [24]

To solve Equation II.27, it is necessary to be more specific about the geometry. We begin with the simplest case of straight rectangular and pin fins of uniform cross section Figure II.5. Each fin is attached to a base surface of temperature $T(0) = T_b$, and extends into a fluid of temperature T_∞.

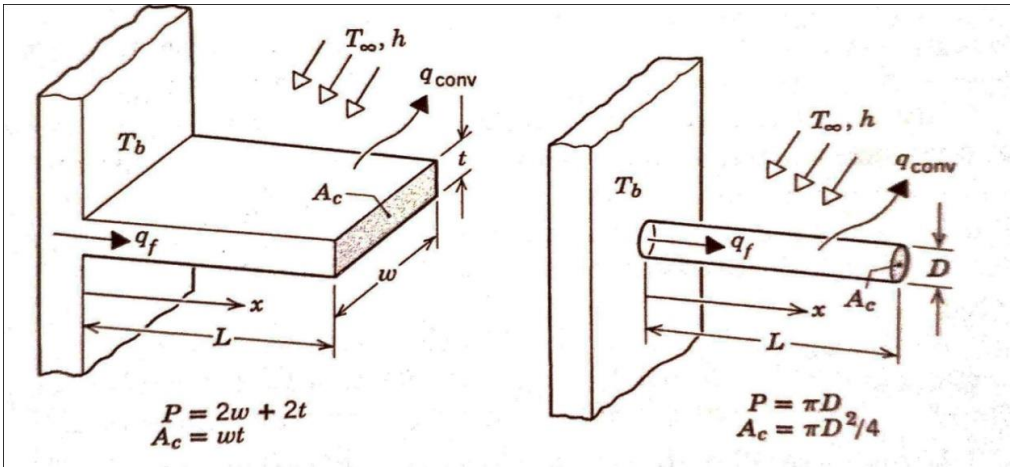

Figure II.5 Straight Fins of Uniform cross section (Rectangular and Pin Fin) [24]

For the prescribed fins, A_c is a constant and $A_s = P\,x$, where A_s is the surface area measured from the base to x and P is the fin perimeter.
Accordingly, with $dA_c/dx = 0$ and $dA_s/dx = P$, Equation II.27, reduces to

$$\frac{d^2T}{dx^2} - \left(\frac{h\,P}{A_c\,k}\right)(T-T_\infty) = 0 \qquad \text{(II.28)}$$

To simplify the form of this equation, we transform the dependent variable by defining an excess temperature Θ as

$$\Theta(x) \equiv T(x) - T_\infty \qquad \text{(II.29)}$$

Since T_∞ is a constant, $d\Theta / dx = dT / dx$. Substituting Equation II.29 into Equation II.28, we then obtain

$$\frac{d^2\theta}{dx^2} - m^2 \Theta = 0 \qquad \text{(II.30)}$$

Where

$$m^2 = \frac{h\,P}{A_c\,k} \qquad \text{(II.31)}$$

Equation II.30 is a linear, homogeneous, second-order differential equation with constant coefficients. Its general solution is of the form

$$\Theta(x) = C_1\, e^{m\,x} + C_2\, e^{-m\,x} \qquad \text{(II.32)}$$

By substitution it may be readily verified that Equation II.32 is indeed a solution to Equation II.30.

To evaluate the constants C_1 and C_2 of Equation II.32, it is necessary to specify appropriate boundary conditions. One such condition may be specified in terms of the temperature at the base of the fin ($x = 0$)

$$\Theta(0) = T_b - T_\infty \equiv \Theta_b \qquad \text{(II.33)}$$

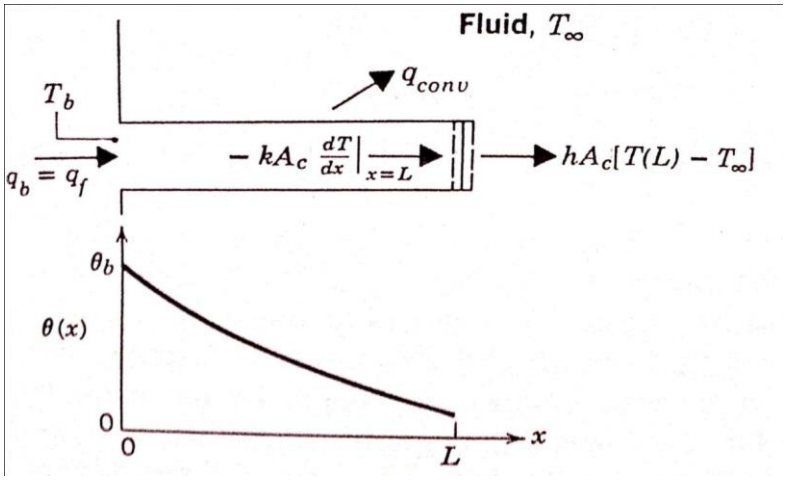

Figure II.6 Conduction and Convection in a Fin of Uniform cross section [24]

The first condition, considers convection heat transfer from the fin tip (x = L) [24]. Applying an energy balance to a control surface about this tip Figure II.6, we obtain

$$h\ A_c\ (T(L) - T_\infty) = -\,k\,A_c \left.\frac{dT}{dx}\right|_{x=L} \qquad \text{(II.34)}$$

or

$$h\,\Theta(L) = -\,k \left.\frac{d\Theta}{dx}\right|_{x=L} \qquad \text{(II.35)}$$

That is, the rate at which energy is transferred to the fluid by convection from the tip must equal the rate at which energy reaches the tip by conduction through the fin. Substituting Equation II.32 into Equations II.33 and II.35, we obtain [24], respectively.

$$\Theta_b = C_1 + C_2 \tag{II.36}$$

And

$$h\,(C_1\, e^{m\,L} + C_2\, e^{-m\,L}) = k\,m\,(C_2\, e^{-m\,L} + C_1\, e^{m\,L}) \tag{II.37}$$

Solving for C_1 and C_2 it may be shown, after some manipulation, that

$$\frac{\Theta}{\Theta_b} = \frac{\cosh m\,(L-x) + \left(\frac{h}{mk}\right)\sinh m\,(L-x)}{\cosh mL + \left(\frac{h}{mk}\right)\sinh mL} \qquad \left(\frac{\Theta}{\Theta_b}\right) \text{ Temperature distribution} \tag{II.38}$$

The form of this temperature distribution is shown schematically in Figure II.6. Note that the magnitude of the temperature gradient decreases with increasing x. This trend is a consequence of the reduction in the conduction heat transfer $q_x\,(x)$ with increasing x due to continuous convection losses from the fin surface.

We are also interested in the total heat transfered by the fin [24]. From Figure II.6 it is evident that the fin heat transfer rate q_f maybe evaluated in two alternative ways, both of which involve use of the temperature distribution. The simpler procedure, and the one which we will use, involves applying Fourier's law at the fin base. That is,

$$q_f = q_b = -\,k\,A_c \left.\frac{dT}{dx}\right|_{x=0} = -\,k\,A_c \left.\frac{d\Theta}{dx}\right|_{x=0} \tag{II.39}$$

However, conservation of energy dictates that the rate at which heat is transferred by convection from the fin must equal the rate at which it is conducted through the base of the fin. Accordingly, the alternative formulation for q_f is

$$q_f = \int_{A_f} h\,\Theta\,(x)\,dA_S \tag{II.40}$$

where A_f is the total, including the tip, fin surface area.

By substitution of Equation II.38 into Equation II.40 would yield Equation II.41

$$q_f = \sqrt{hPkA_c}\;\Theta_b\;\frac{\sinh mL + \left(\frac{h}{mk}\right)\cosh mL}{\cosh mL + \left(\frac{h}{mk}\right)\sinh mL} \tag{II.41}$$

With q_f is the fin heat transfer rate

II.4 Validity of the Fin:

II.4.1 Biot number:

We will frequently have occasion to apply the conservation of energy requirement Equation II.42 at the surface of the fin, reduces to II.43 from Figure II.6 [24]

$$\dot{E}_{in} - \dot{E}_{out} = 0 \qquad \text{(II.42)}$$

$$hA\,(T(L) - T_\infty) = (T_b - T(L))\frac{KA}{L} \qquad \text{(II.43)}$$

We then obtain

$$\frac{Tb - T(L)}{T(L) - T\infty} = \frac{(L/KA)}{(1/hA)} = \frac{R_{cond}}{R_{conv}} = \frac{hL}{K} \equiv Bi \qquad \text{(II.44)}$$

The quantity (h.L/k) appearing in Equation II.44 is a dimensionless parameter. It is termed the Biot number, and it plays a fundamental role in conduction problems that involve surface convection effects. The Biot number provides a measure of the temperature drop in the solid relative to the temperature difference between the surface and the fluid. Note especially the conditions corresponding to Bi << 1. The results suggest that, for these conditions, it is reasonable to assume a uniform temperature distribution within a solid at any time during a transient process. This result may also be associated with interpretation of the Biot number as a ratio of thermal resistances, Equation II.44. If Bi << 1, the resistance to conduction R_{cond} in the solid is much less than the resistance to convection R_{conv} across the fluid boundary layer. [24]

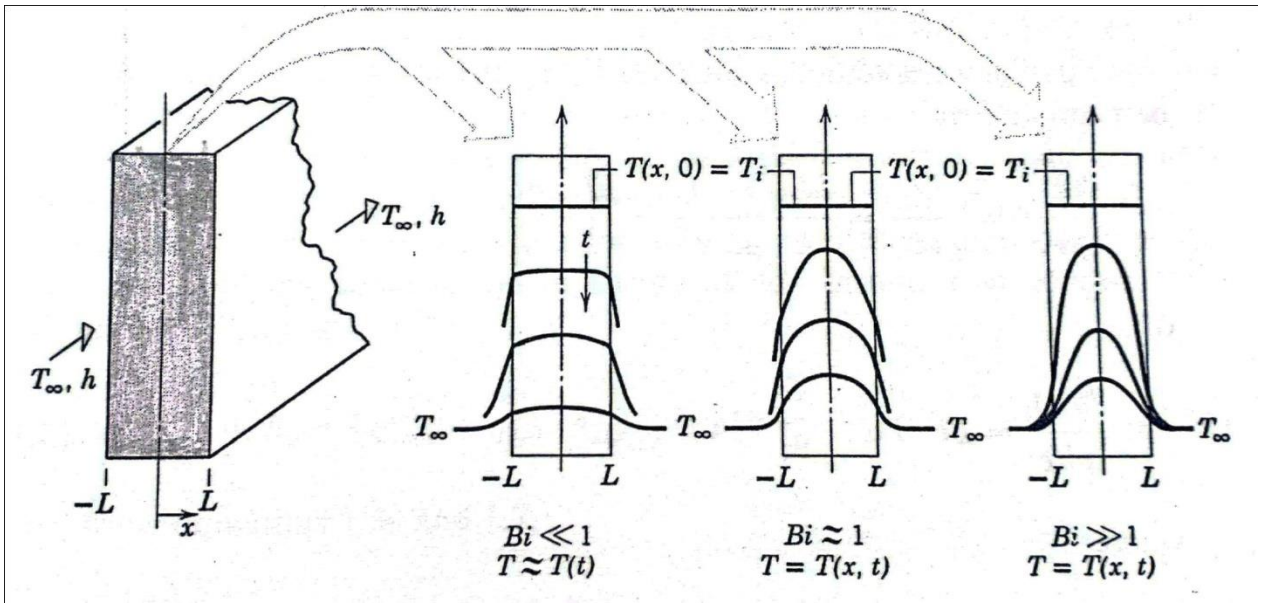

Figure II.7 Effect of Biot number on steady-state Temperature distribution in a plane wall with surface convection [24]

The three conditions are shown in Figure II.7. For Bi << 1 the temperature gradient in the solid is small and T(x, t) ≈ T(t). Virtually all the temperature difference is between the solid and the fluid, and the solid temperature remains nearly uniform as it decreases to T_∞. For moderate to large values of the Biot number, however, the temperature gradients within the solid are significant.

Hence T = T(x, t). Note that for Bi >> 1, the temperature difference across the solid is much larger than that between the surface and the fluid. So for the valuable fin we should to calculate the Biot number and see if the condition bellow is satisfied [24].

$$Bi \equiv \frac{hL_c}{K} < 0.1 \qquad \text{(II.45)}$$

With L_c is the ratio of the solid's volume to surface area, $L_c \equiv V/A_s$

For this, it is necessary to determine the convection heat coefficient value, of which varies according to several application conditions.

II.5 Heat Transfer Coefficient for Free Convection:

For convection heat transfer calculation, Nusselt number is determine by:

$$Nu_L = \frac{h*L}{k_a} \Leftrightarrow h = \frac{Nu_L * k_a}{L} \qquad \text{(II.46)}$$

II.5.1 Nusselt number: Basic dimensionless convective heat transfer coefficient (ration of convection heat transfer to conduction in a fluid slab of thickness L) [25].

$Nu = 0.13\ Ra^{1/3}$ $Ra_L < 2*10\text{^}8$ (Laminer mode) (II.47)

$Nu = 0.16\ Ra^{1/3}$ $5*10\text{^}8 < RaL < 10\text{^}11$ (Turbulent mode) (II.48)

For that, it is necessary to evaluate Rayleigh number:

II.5.2 Rayleigh number: Modified Grashof number [25].

$$Ra_L = Gr_L * Pr \qquad \text{(II.49)}$$

II.5.3 Grashof number: Ratio of buoyancy to viscous forces [25].

$$Gr_L = \frac{g*\beta*(T_S - T_\infty)*L^3}{\nu^2} \qquad \text{(II.50)}$$

II.5.4 Prandtl number: Ration of molecular momentum and thermal diffusivities [25].

$$Pr = \frac{\mu C_p}{K} = \frac{\nu}{\alpha} \qquad \text{(II.51)}$$

Conclusion:

In this chapter, we wrote the heat balance for the air collector without fins and with fins in general, and the heat balance for the fin in particular, in order to apply them and use them in the next chapter, for boundary conditions and their calculation for the simulations.

CHAPTER III

MODELING AND CFD ANALYSIS

Introduction:

In this section, the study in more details and the air collector characteristic that is going to be modeled by using ANSYS Fluent 6.3 and 19.2.

First of all, after choosing an experimental work in the state of Adrar [26] about an indirect solar dryer, in order to choose an optimal dimensions and appropriate conditions of the air collector, and compare our work with it. which is, changing the fin thickness, fin material, and fin position.

III.1 Computational Fluid Dynamics:

Computational fluid dynamics or CFD is the analysis of systems involving fluid flow, heat transfer and associated phenomena such as chemical reactions by means of computer-based simulation. CFD is part of computational mechanics, which in turn is part of simulation techniques. Simulation is used by engineers and physicists to forecast or reconstruct the behavior of an engineering product or physical situation under assumed or measured boundary conditions (geometry, initial states, loads, etc.). [27]

III.2 Fluid Governing Equations:

The cornerstone of computational fluid dynamics is the governing equations of fluid dynamics- the continuity equation, momentum equation and energy equation. These equations speak physics. They are the mathematical statements of three fundamental physical principles upon which all of fluid dynamics is based: [27]

- Conservation of mass
- Conservation of momentum
- Conservation of energy

III.3 Naiver-Stokes Equations:

III.3.1 Continuity Equation:

The continuity equation describes the conservation of mass. It is given by [28]

$$\frac{\partial \rho}{\partial t} = -(\nabla . \rho V) \qquad \text{(III.1)}$$

III.3.2 Momentum Equation:

The momentum equation describes the law of conservation of momentum which states that the net force acting on a mass is equal to the change in momentum in that direction. [25]

$$\frac{\partial \rho V_x}{\partial t} + \frac{\partial (\rho V_x V_x)}{\partial x} + \frac{\partial (\rho V_y V_x)}{\partial y} + \frac{\partial (\rho V_z V_x)}{\partial z} = \rho g_x - \frac{\partial P}{\partial x} + \frac{\partial}{\partial x}\left(\mu_e \frac{\partial V_x}{\partial x}\right) + \frac{\partial}{\partial y}\left(\mu_e \frac{\partial V_x}{\partial y}\right) + \frac{\partial}{\partial z}\left(\mu_e \frac{\partial V_x}{\partial z}\right) \qquad \text{(III.2)}$$

$$\frac{\partial \rho V_y}{\partial t} + \frac{\partial (\rho V_x V_y)}{\partial x} + \frac{\partial (\rho V_y V_y)}{\partial y} + \frac{\partial (\rho V_z V_y)}{\partial z} = \rho g_y - \frac{\partial P}{\partial y} + \frac{\partial}{\partial x}\left(\mu_e \frac{\partial V_y}{\partial x}\right) + \frac{\partial}{\partial y}\left(\mu_e \frac{\partial V_y}{\partial y}\right) + \frac{\partial}{\partial z}\left(\mu_e \frac{\partial V_y}{\partial z}\right) \qquad \text{(III.3)}$$

$$\frac{\partial \rho V_z}{\partial t} + \frac{\partial (\rho V_x V_z)}{\partial x} + \frac{\partial (\rho V_y V_z)}{\partial y} + \frac{\partial (\rho V_z V_z)}{\partial z} = \rho g_z - \frac{\partial P}{\partial z} + \frac{\partial}{\partial x}\left(\mu_e \frac{\partial V_z}{\partial x}\right) + \frac{\partial}{\partial y}\left(\mu_e \frac{\partial V_z}{\partial y}\right) + \frac{\partial}{\partial z}\left(\mu_e \frac{\partial V_z}{\partial z}\right) \qquad \text{(III.4)}$$

Where:

g_x, g_y, g_z = components of acceleration due to gravity

ρ = mass volume and μ_e = effective viscosity

III.3.3 Energy Equation:

One of the most fundamental laws in nature, First Law of Thermodynamics, also known as, conservation of energy principle, provides a basis for studying the relations among energy and energy interactions. It states that "Energy can neither be created nor destroyed, it can only be changed from one form to another". Conservation of energy principle for any system can simply be expressed as

$$\frac{\partial}{\partial t}(\rho.H) + \nabla.(\rho.v.H) = \nabla.(k\nabla T) + s \quad [28] \qquad \text{(III.5)}$$

where H = enthalpy

ρ = Density

v = fluid velocity

S = source term

III.4 Assumptions:

- Steady state for the simulation work.
- Temperature for the absorber plate is imposed Uniform.
- Fins inlet Heat flux is Uniform.
- Surface radiation effects are negligible. [25]
- Incompressible flow.
- Fin-absorber resistance is negligible.
- The effect of gravity is weak for air

III.4.1 Assumptions Applying:

III.4.1.1 Continuity Equation will be:

$$(\nabla.\rho V) = 0 \qquad \text{(III.6)}$$

III.4.1.2 Momentum Equation will be:

$$\rho\left(\frac{\partial V_z}{\partial t} + \frac{\partial(V_x V_x)}{\partial x} + \frac{\partial(V_y V_x)}{\partial y} + \frac{\partial(V_z V_x)}{\partial z}\right) = -\frac{\partial P}{\partial x} + \frac{\partial}{\partial x}\left(\mu_e \frac{\partial V_x}{\partial x}\right) + \frac{\partial}{\partial y}\left(\mu_e \frac{\partial V_x}{\partial y}\right) + \frac{\partial}{\partial z}\left(\mu_e \frac{\partial V_x}{\partial z}\right) \qquad \text{(III.7)}$$

$$\rho\left(\frac{\partial V_y}{\partial t} + \frac{\partial(V_x V_y)}{\partial x} + \frac{\partial(V_y V_y)}{\partial y} + \frac{\partial(V_z V_y)}{\partial z}\right) = -\frac{\partial P}{\partial y} + \frac{\partial}{\partial x}\left(\mu_e \frac{\partial V_y}{\partial x}\right) + \frac{\partial}{\partial y}\left(\mu_e \frac{\partial V_y}{\partial y}\right) + \frac{\partial}{\partial z}\left(\mu_e \frac{\partial V_y}{\partial z}\right) \qquad \text{(III.8)}$$

$$\rho\left(\frac{\partial V_z}{\partial t} + \frac{\partial(V_x V_z)}{\partial x} + \frac{\partial(V_y V_z)}{\partial y} + \frac{\partial(V_z V_z)}{\partial z}\right) = -\frac{\partial P}{\partial z} + \frac{\partial}{\partial x}\left(\mu_e \frac{\partial V_z}{\partial x}\right) + \frac{\partial}{\partial y}\left(\mu_e \frac{\partial V_z}{\partial y}\right) + \frac{\partial}{\partial z}\left(\mu_e \frac{\partial V_z}{\partial z}\right) \qquad \text{(III.9)}$$

III.4.1.3 Energy Equation will be:

$$\rho\left(\frac{\partial(H)}{\partial t}+\nabla.(v.H)\right)=k.\nabla.(\nabla T) \qquad \text{(III.10)}$$

III.5 Steps in Solving CFD Problem: [27]

1. Define the modeling goals.
2. Create the model geometry.
3. Generate the mesh.
4. Set up the solver and physical models.
5. Compute and monitor the solution.

III.6 Geometry creation:

The air collector geometry used during the entire work is not fully detailed model: parts like glass cover, air gap is excluded from the model. the effects of most of these simplifications are negligible and essential to reduce model simulation time.

III.6.1 First case: without fins

The body of the collector is composed of an absorbent plate 5 millimeters of thickness, and a frame for insulation; their assembly creates the duct where the circulating incoming air is heated. The duct has a parallelepiped shape of 95 × 100 × 4 cm^3 shown in Figure III.1.

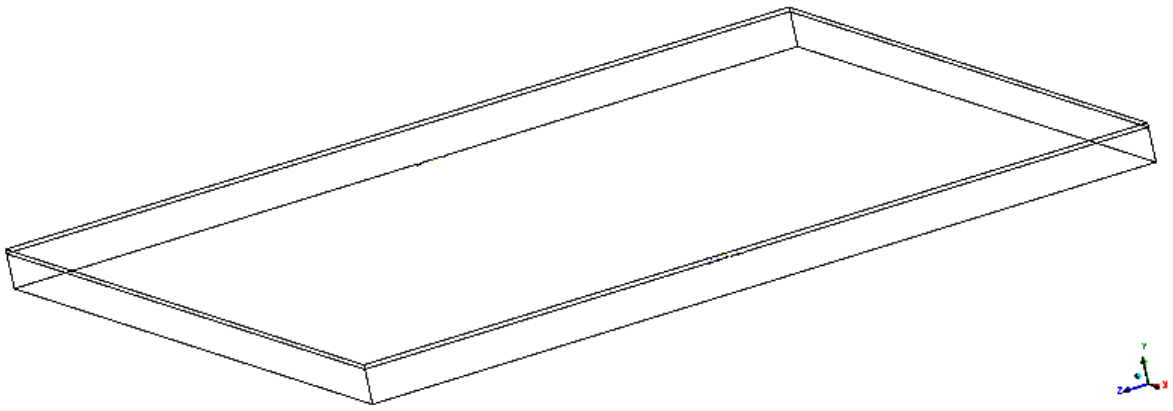

Fig III.1 Geometry of the Air Collector without Fins

III.6.2 Second case: with fins

The same geometry just adding fins under the absorber plate, and change the fin characteristics shown in figure III.2.

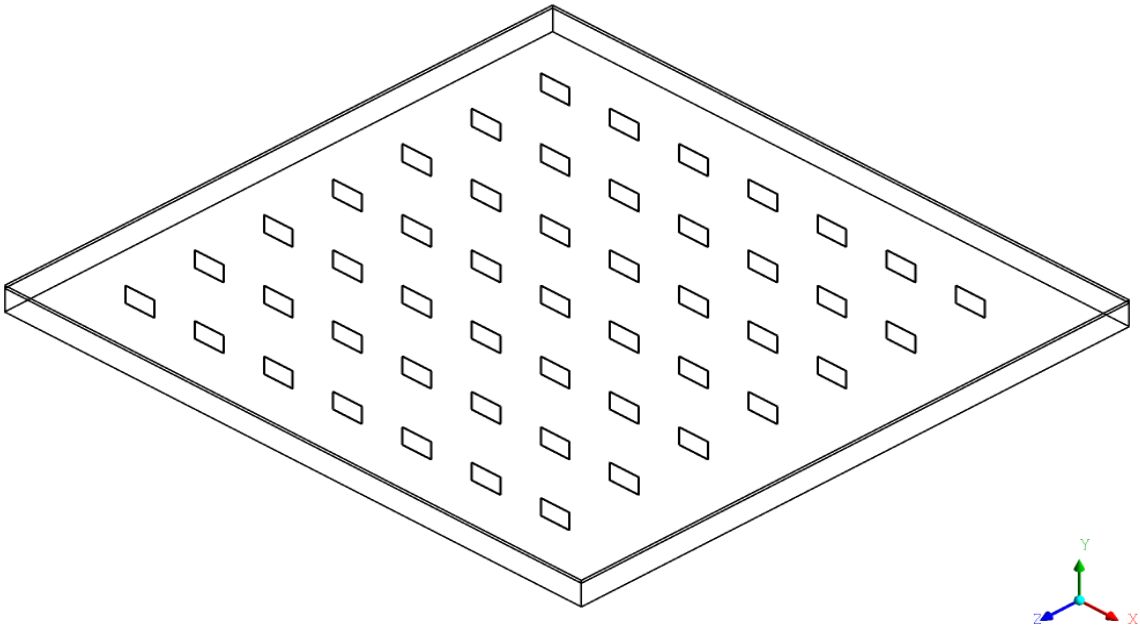

Figure III.2 Geometry of the Air Collector with Fins

III.7 Analysis of Air Collector with and without Fins:

In this work, the modeling of the geometry is done using Gambit 2.4.6 and imported to ANSYS FLUENT 2.6 and 19.2 and the meshing, solver, material selection, boundary conditions, etc are done step by step and the results are analyzed.

III.7.1 Mesh generation:

Without fins:

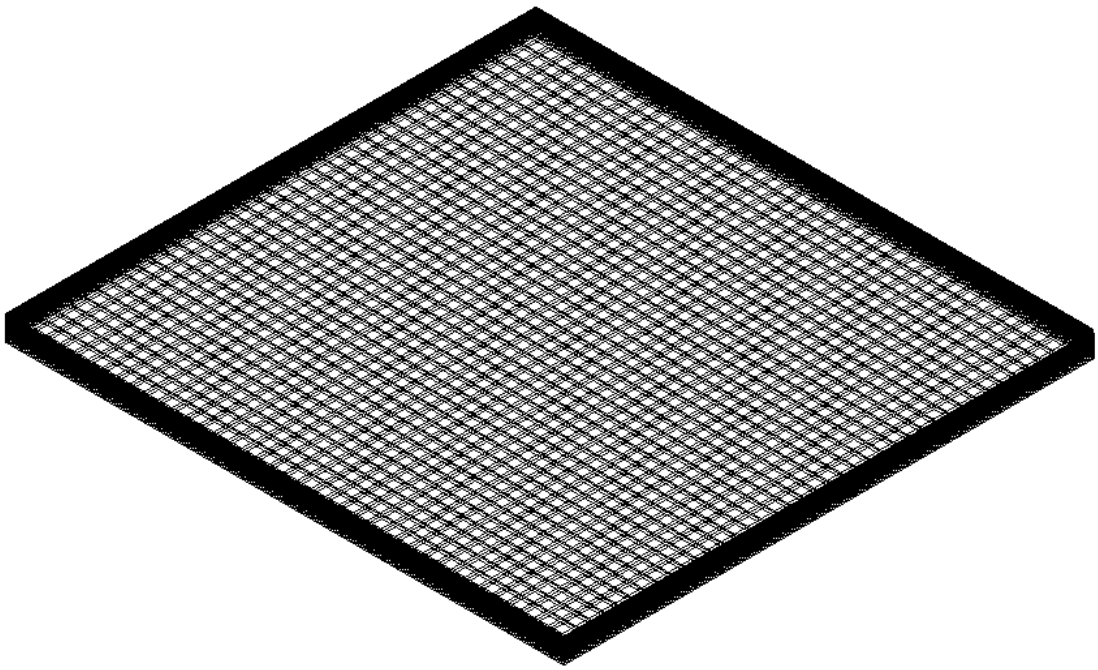

Figure III.3 Initial meshing of the Air Collector without Fins

the mesh used in the development study consisted of approximately 76500 cells and was created in Gambit 2.4.6.

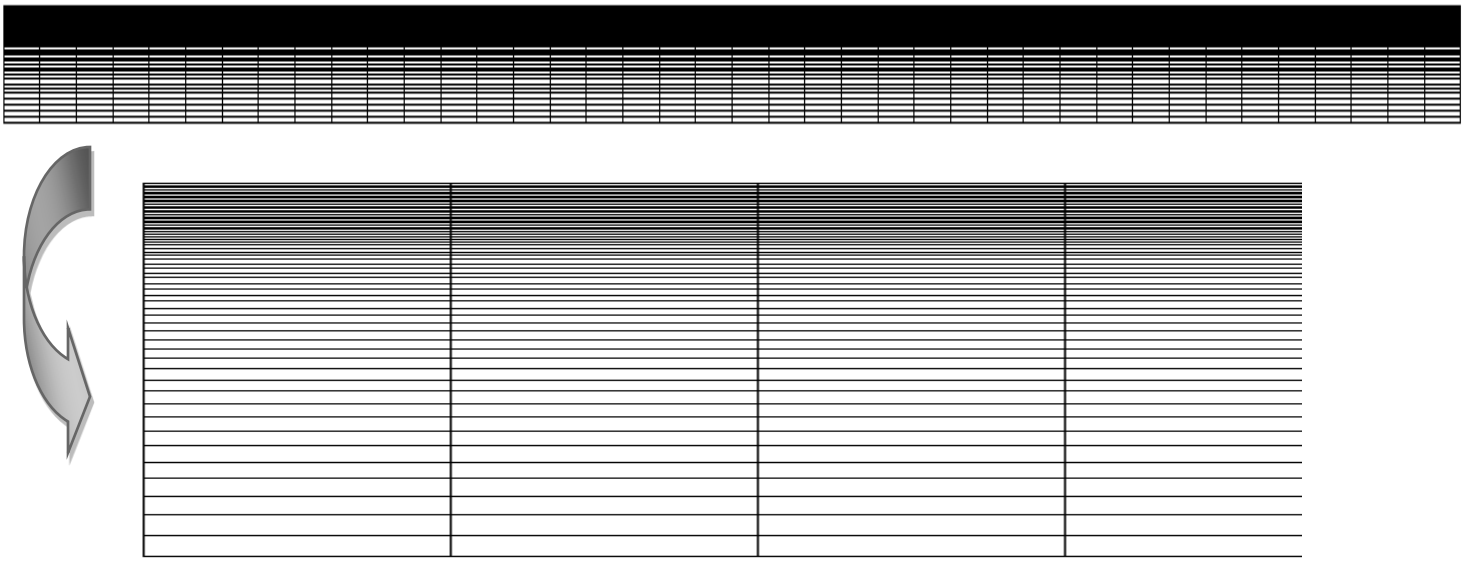

Figure III.4 Side section for mesh of the Air Collector without Fins

With fins:

The mesh consisted about 344000 cells, and was created too in Gambit 2.4.6.

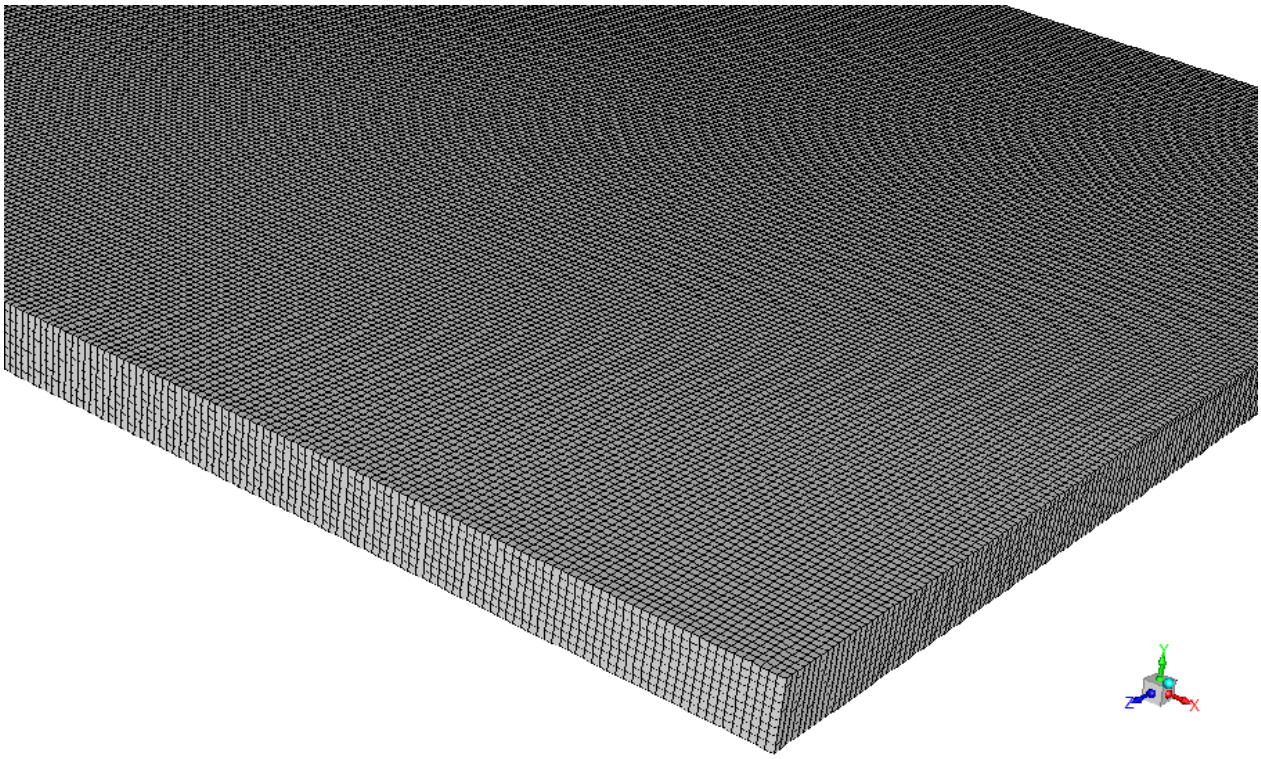

Figure III.5 Initial meshing of the Air Collector with Fins

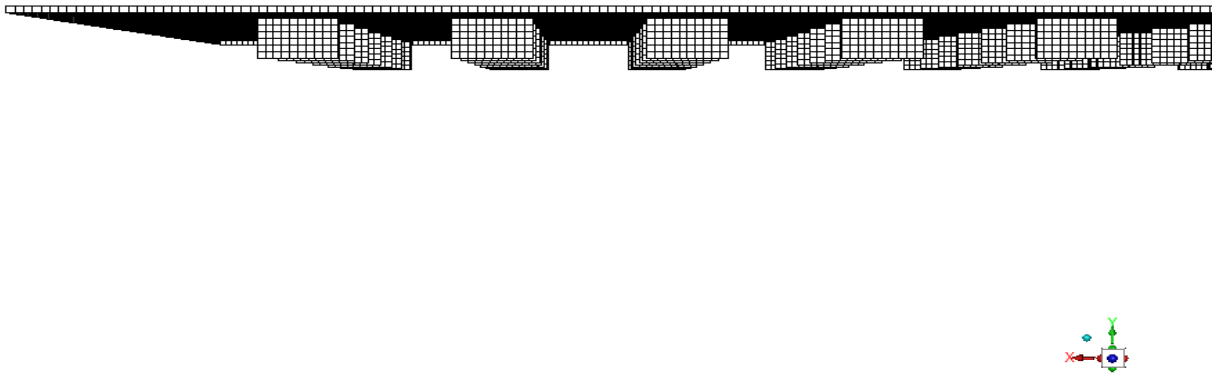

Figure III.6 Meshing of the Air Collector with Fins

III.7.2 Solver, Material Selection and Boundary Condition:

III.7.2.1 Solver:

The solver used in this project, as mentioned earlier, has been FLUENT version 6.3 and 19.2. The specified solver settings were:

Table III.1 Solver used throughout the thesis.

Physical Parameters	Values
Models	Energy: on Viscous K – Epsilon K – Epsilon Standard wall fin

III.7.1.2 Boundary Condition:

Two different thermal boundary conditions were used consistently throughout this dissertation:

Heat Flux and Temperature.

- The heat-flux boundary condition allows us to set surfaces as constant energy sources by specifying a heat flux in W/m^2. This boundary setting was used for fins conditions (uniform heat flux) and when setting unimportant surfaces as adiabatic (insulation).
- The temperature boundary condition allows us to set surfaces as constant temperature sources in k. This boundary setting was only used for absorber plate (uniform temperature).

Without fins:

Table III.2 Boundary Condition of the most important surfaces in the study without Fins

BC	type	material	temperature	Wall thickness(mm)
Abs plate	Temperature	aluminum	361	5
Insulator	Heat flux	Rock flax	0	/
Air inlet	Temperature	Air	303	/
Air outlet	Out flow	Air	Calculate	/

With fins:

Table III.3 Boundary Condition of the most important surfaces in the study with Fins

BC	type	material	temperature	Wall thickness(mm)
Abs plate	Temperature	aluminum	361	5
Insulator	Heat flux	Rock flax	0	/
Air inlet	Temperature	Air	303	/
Air outlet	Out flow	Air	Calculate	/
Fin base	Temperature	aluminum	361	Change
Fin walls	Convection	aluminum	Change	Change

The materials set in all simulations in this work, was mentioned, in the Table III.4.

Table III.4 Material data used throughout the thesis.

Material	Density [kg/m3]	Cp [J/kg K]	Thermal Conductivity [W/m K]
aluminum	2719	871	240
Air	1.225	1006.43	0.0242
Insulator	20	700	0.03

III.8 Summary of Simulation Work:

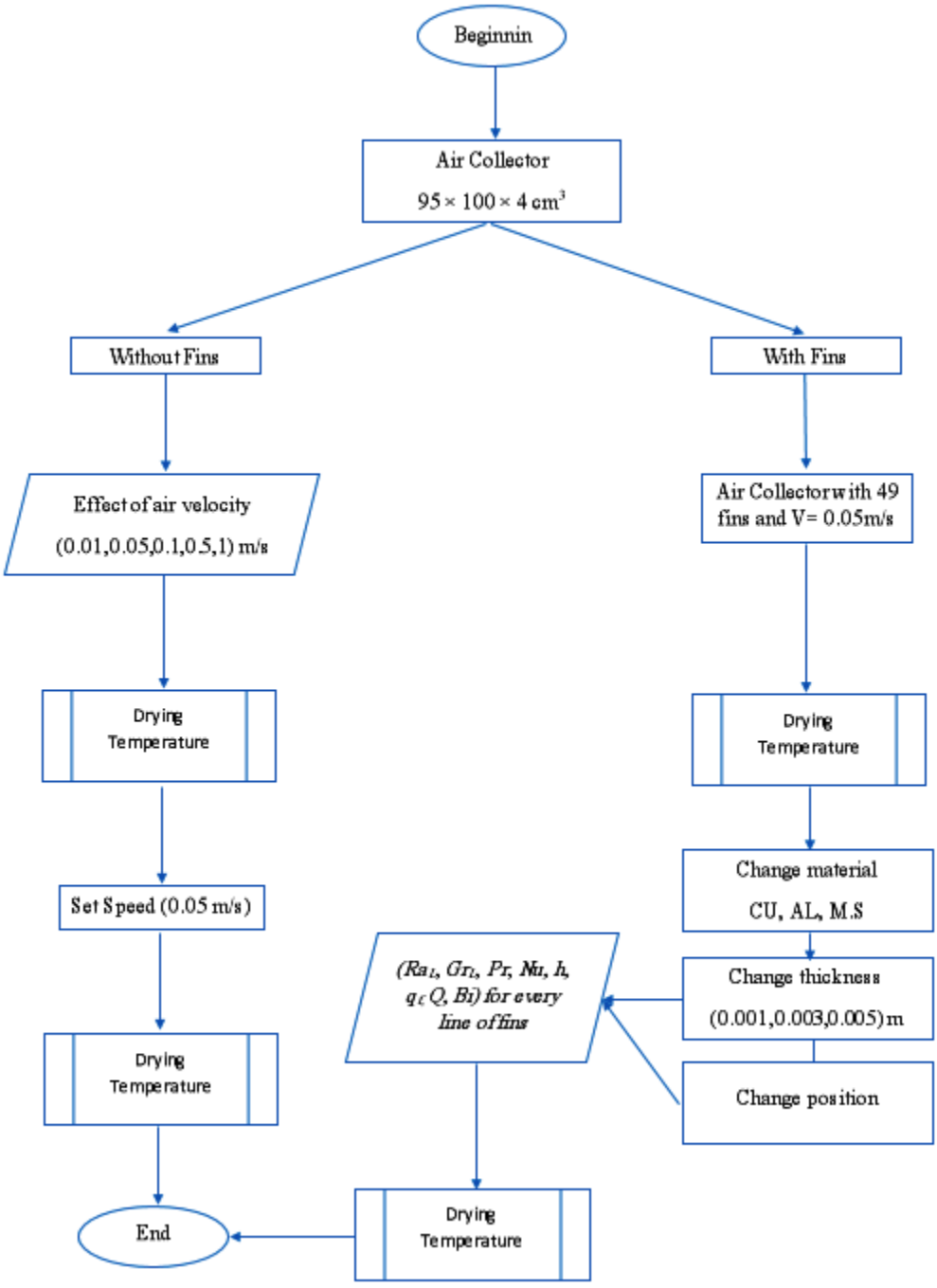

Figure III.7 Simulation work flowchart

Conclusion:

Two types of cases were simulated during this dissertation. Firstly, an attempt to simulate the applied work that was conducted in the state of Adrar and obtain similar results. Secondly, the work, which is related to adding fins to the air collector, and saw the effect of properties on them, and compared it with the results obtained from the first simulation, and with the experimental work that applied in Adrar state. and all that shown in the next chapter.

CHAPTER IV

RESULTS AND DISCUSSIONS

Introduction:

This chapter, present the results obtained from the simulation and engage in a detailed discussion of their significance and implications.

IV.1 Temperature measurement:

we choose 3 lines (near absorber, middle air volume and near insulator) for the temperature measurement from the beginning to the end (drying temperature) of the air collector, shown in figure IV.1

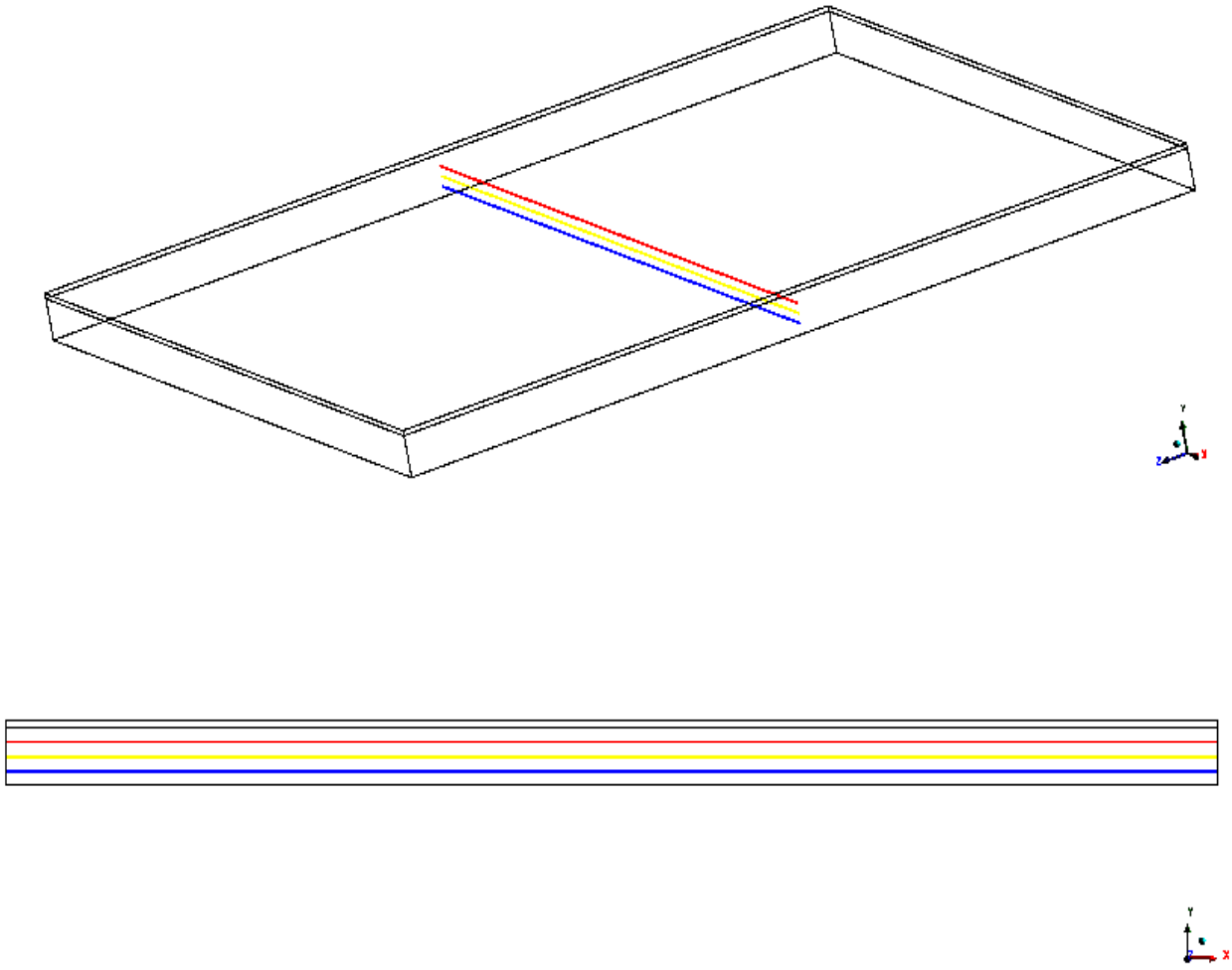

Figure IV.1 Air Collector with the 3 lines (near absorber, middle air volume and near insolent)

IV.2 Air collector without fins:

IV.2.1 Mesh adapting effect:

To study the effect of mesh adapting, the simulation is done for 3 elements shown in figure IV.2.

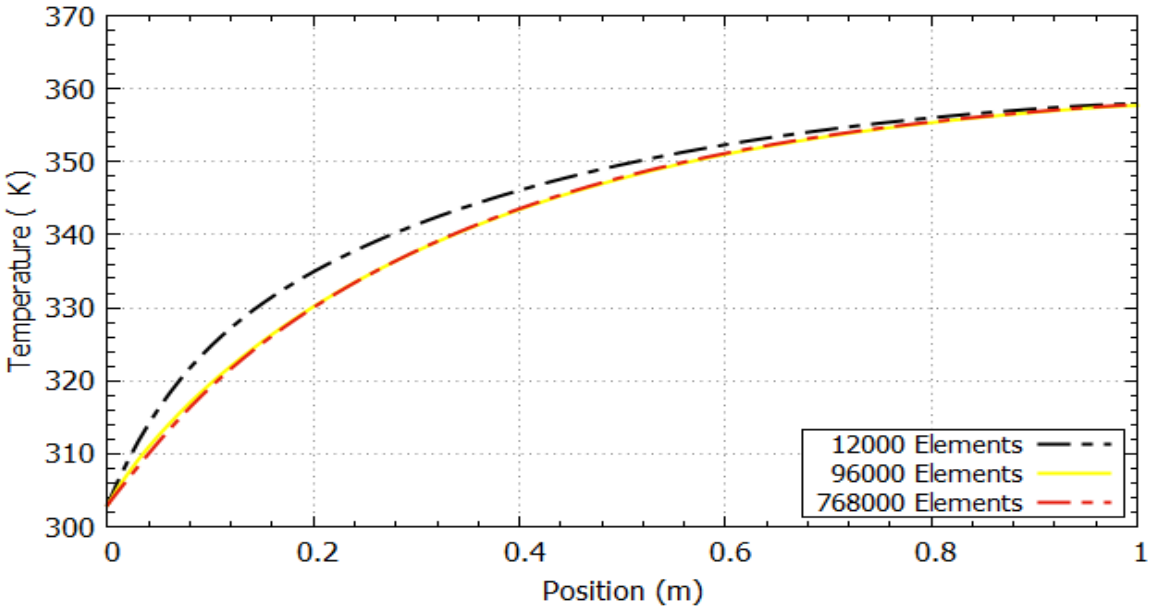

Figure IV.2 Mesh adapting

The figure IV.2 represents the mesh number's effect on the temperature variation. It's clearly that for different cells, there is the same outlet temperature. The yellow and the red lines are the same so that mean the optimal cells number between those lines. And cause the difficult simulation and the time, we used the cells number between the black and the yellow line.

IV.2.2 Air velocity effect: in this part, the effect of inlet air velocity is study for (0.01, 0.05, 0.1, 0.5 and 1 m/s).

0.01 m/s air velocity:

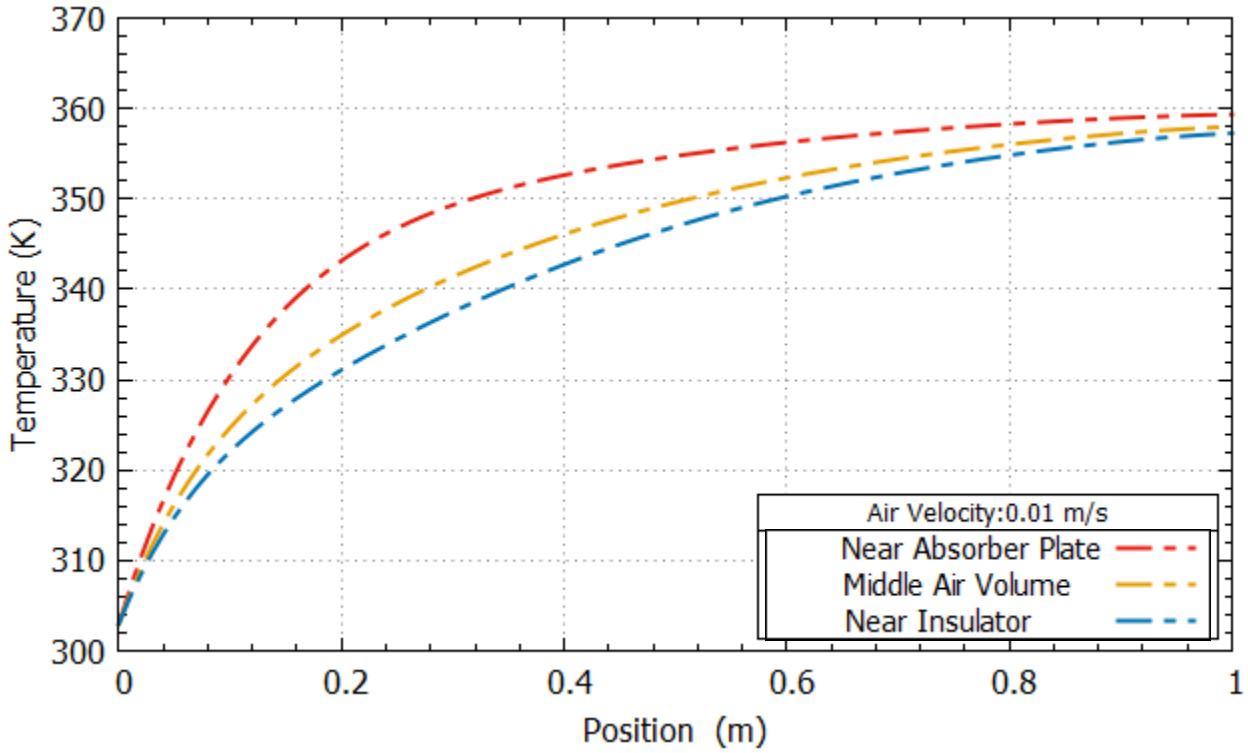

Figure IV.3 The Temperature distribution for the Air Collector without Fins at different Positions

- **0.05 m/s air velocity:**

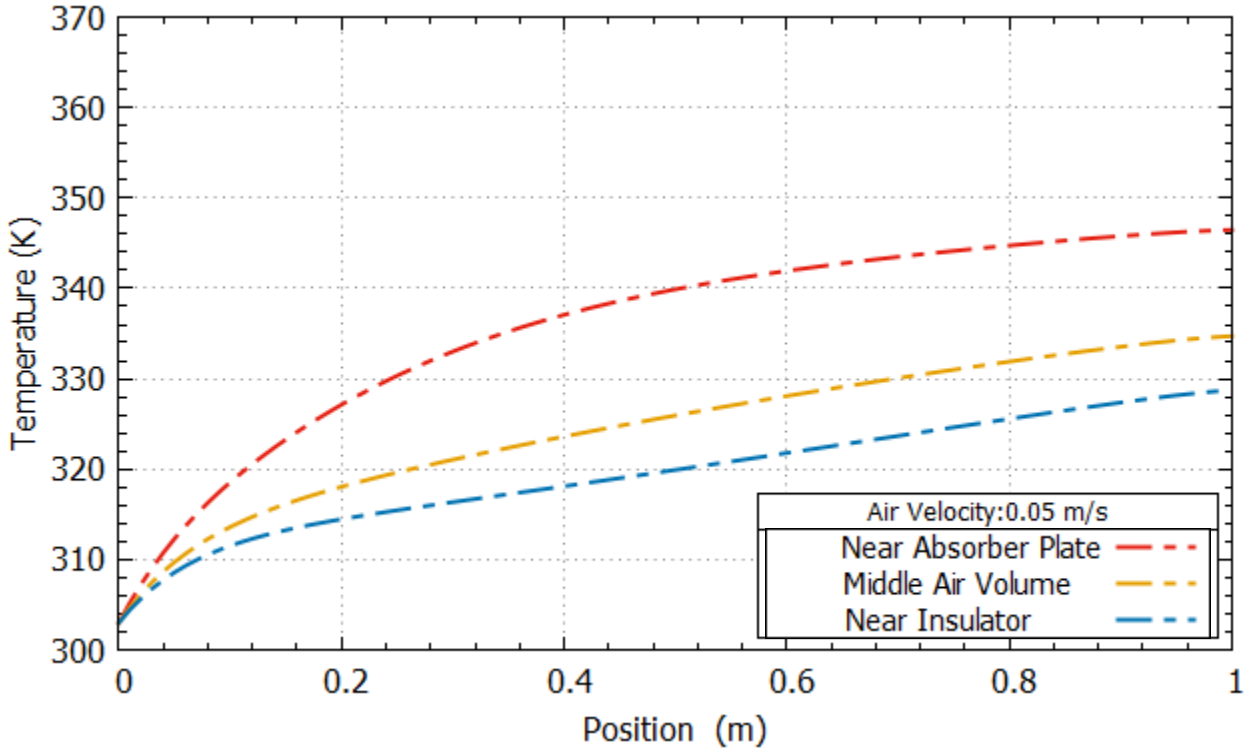

Figure IV.4 The Temperature distribution for the air collector without Fins at different positions

- **0.1 m/s air velocity:**

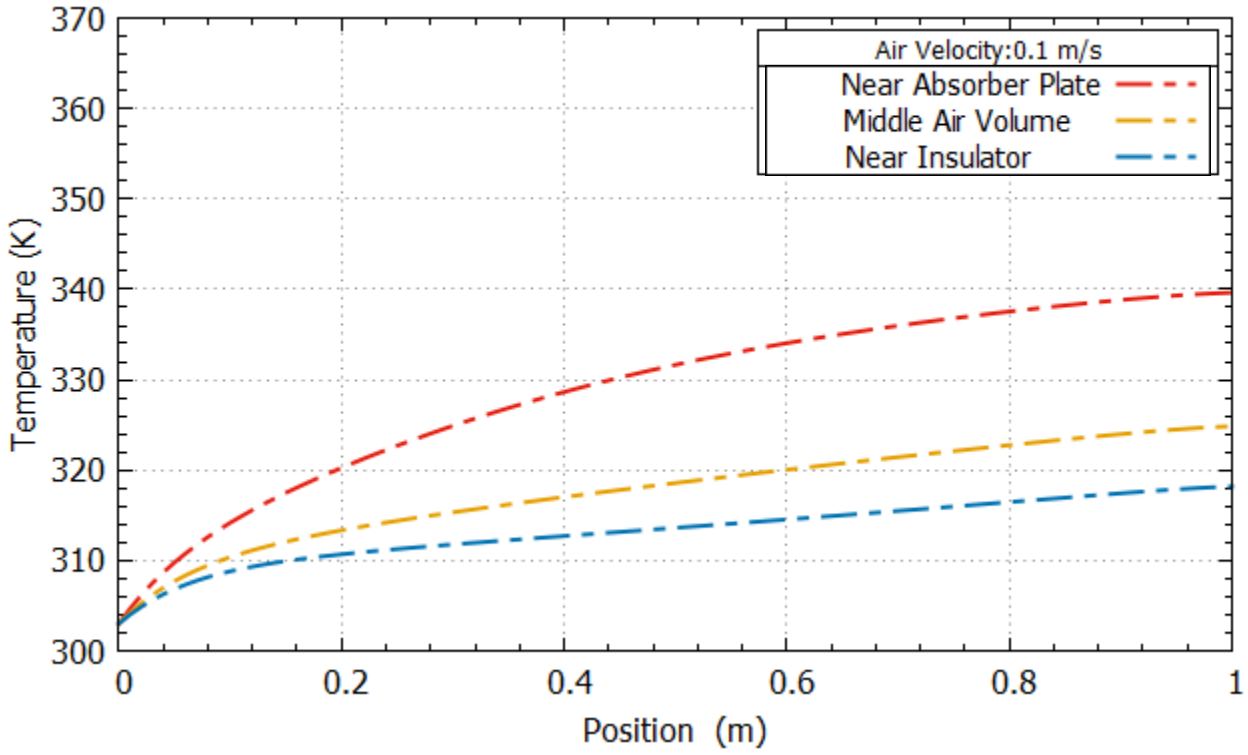

Figure IV.5 The Temperature distribution for the air collector without Fins at different Positions

- **0.5 m/s air velocity:**

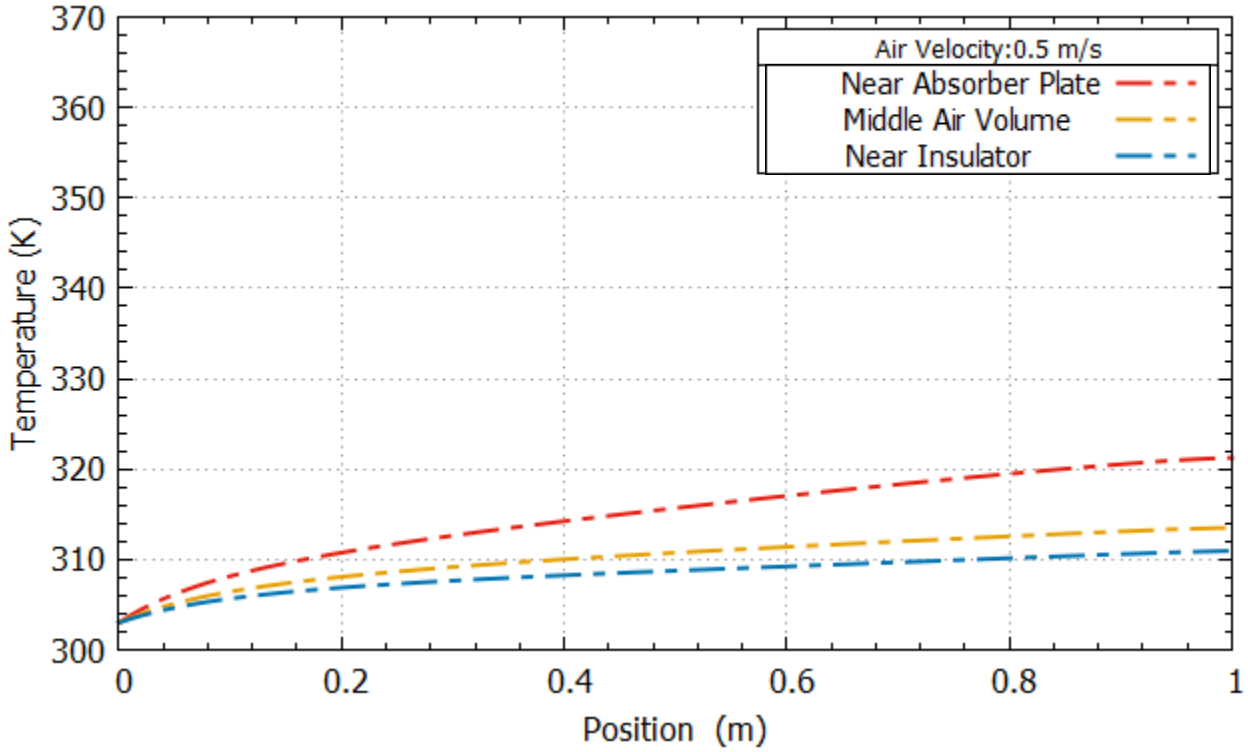

Figure IV.6 The Temperature distribution for the air collector without Fins at different Positions

- **1 m/s air velocity:**

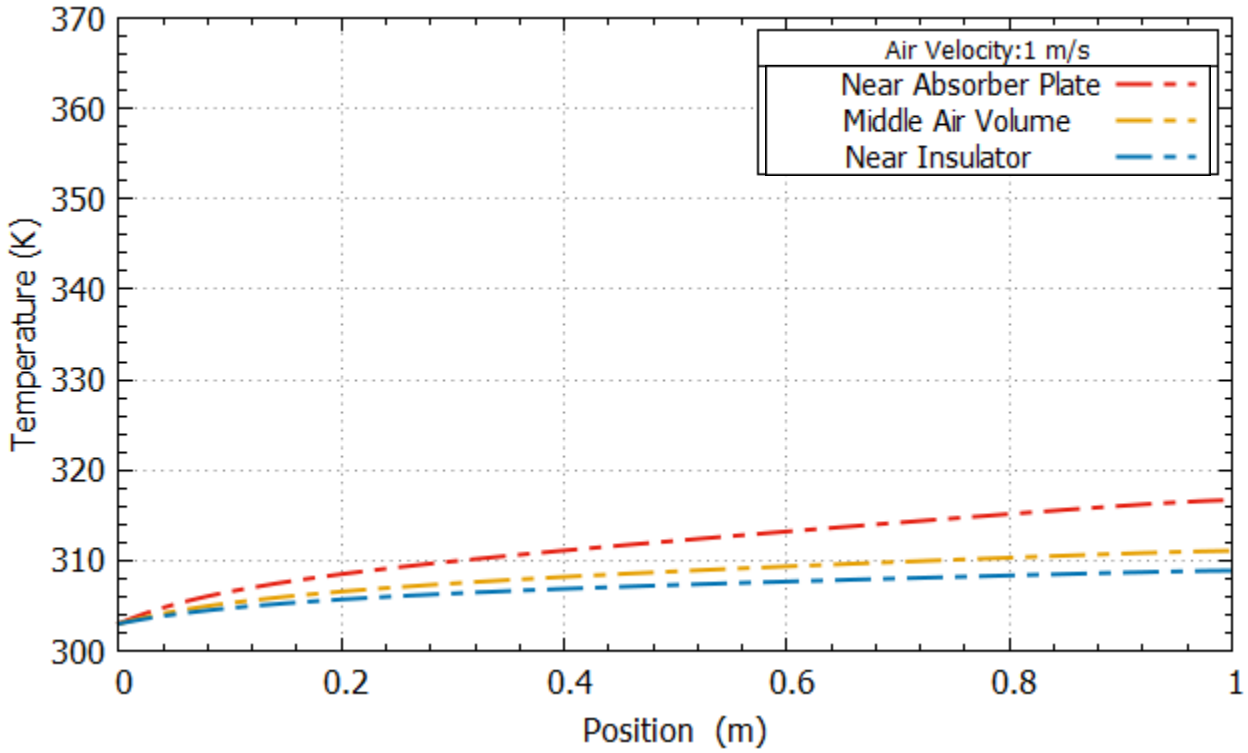

Figure IV.7 The Temperature distribution for the air collector without Fins at different Positions

Figure IV.3 to IV.7 show the temperature distribution of different air velocity (0.01,0.05,0.1,0.5 and 1) m/s at different positions. As it is evident in Figure IV.3 – IV.7, with the increase in air velocity, we can see a decrease in the temperature directed to the drying room, this is due to the smooth surface and the insufficient residence time at higher air velocities in absorber plat wall, which reduced the convective heat transfer.

.

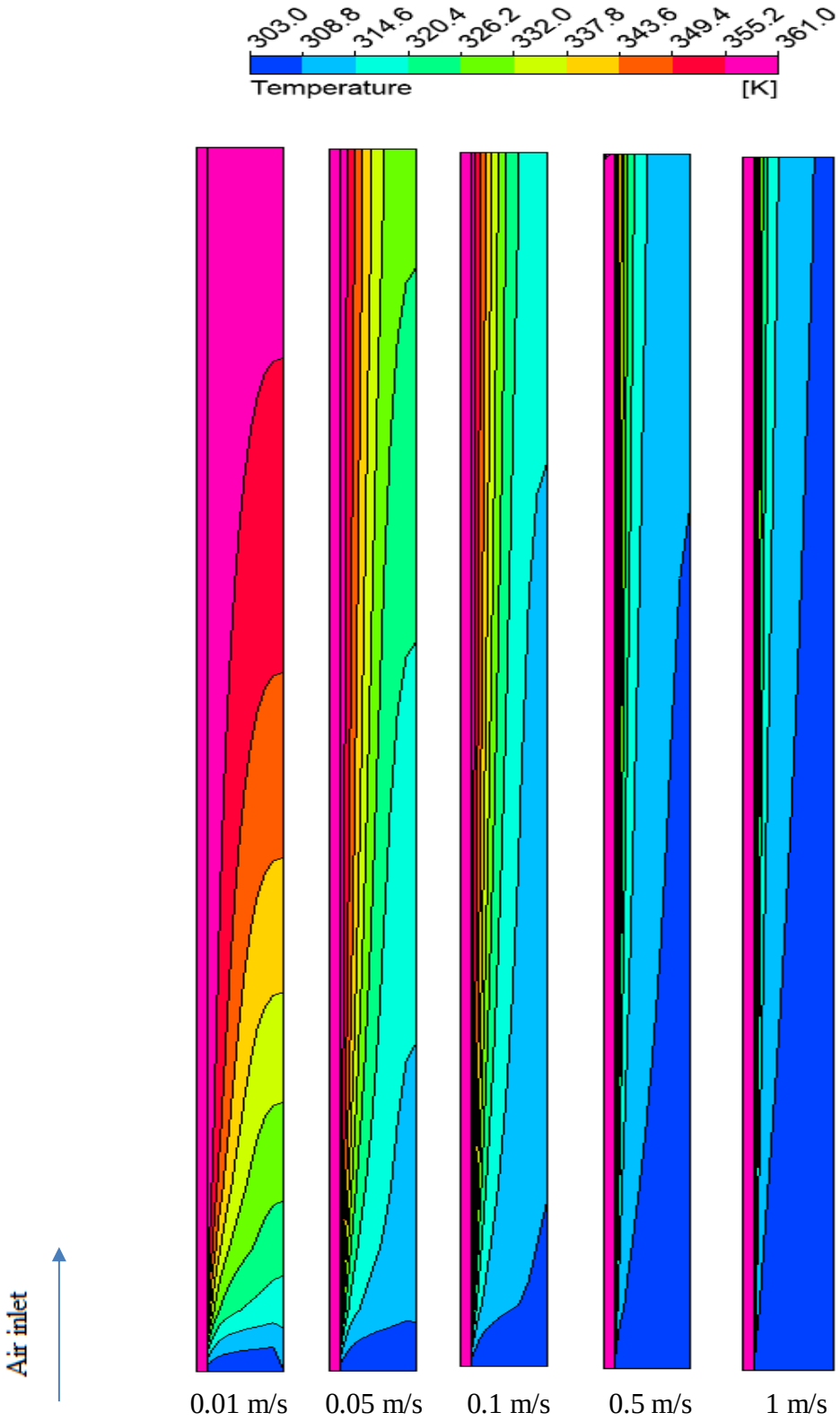

Figure IV.8 Vertical section of Temperature contours for the Air Collector without Fins

For the next figure, figure IV.8 represent the temperature distribution in the air collector at different positions. As it is evident, the average temperature is lower for the base area of the air inside the collector. By moving upward, the average temperature increases gradually and sees the highest value at the top of the air next to the absorber plat. This is due to the density of the air, as the air temperature rises, it becomes more and more lighter, for that the air rises to the top of the air volume

Note: After selecting the simulation with an air velocity of 0.05 m/s, her contour shown in figure IV.9.in order to compare it with a finned collector for the same air velocity.

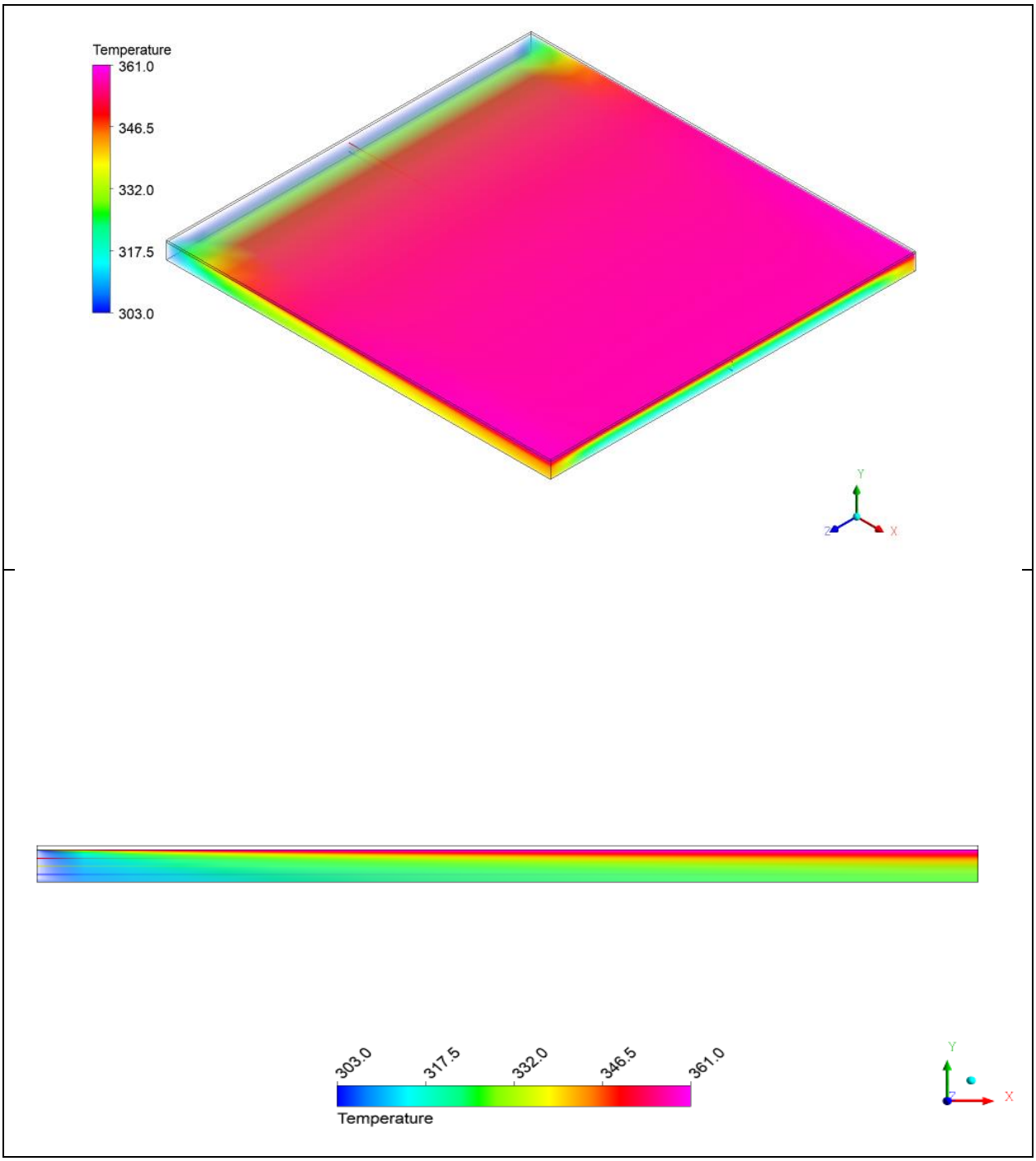

Figure IV.9 Temperature contour of the Air Collector at Air Velocity of 0.05 m/s

IV.3 Air collector with fins:

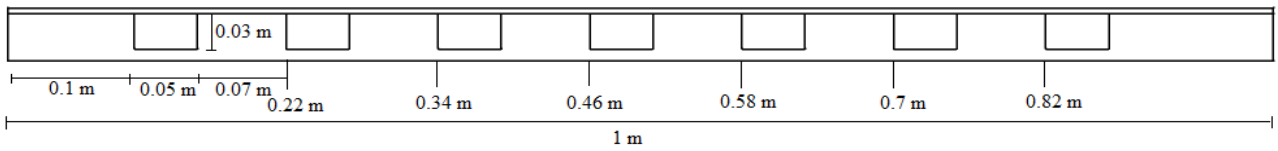

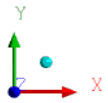

Figure IV.10 Air Collector with Fins sizing

Air collector with the fins sizing is shown in figure IV.10, as we can see, there is 7 lines of fins, we calculated the heat transfer coefficient h for every line for the input in the simulation, shown in figure IV.11.

IV.3.1 Heat Transfer Coefficient: in this part, the heat transfer is calculating for every fin lines for the simulation input.

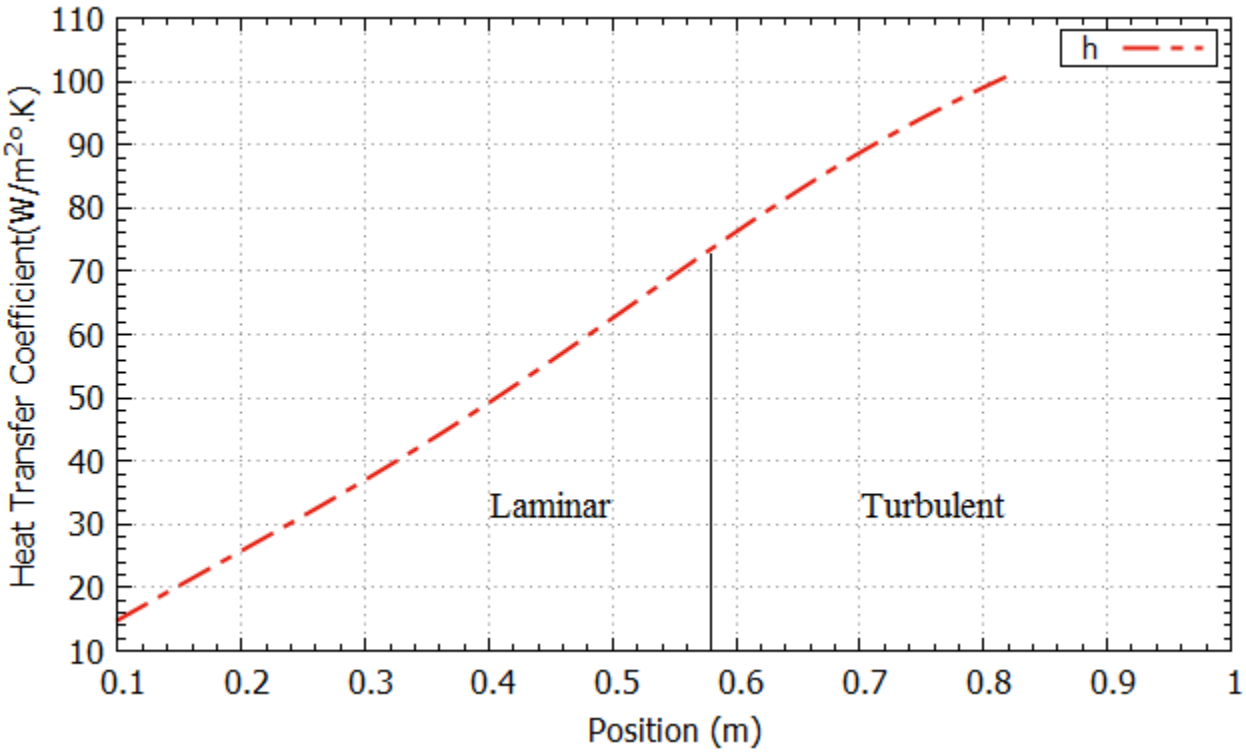

Figure IV.11 Heat Transfer Coefficient for Fin lines

Figure IV.11 show the heat transfer coefficient variation at different positions. As the air enters and moves along the collector, we see an increase in the heat transfer coefficient, that due to its high temperature and entering the turbulent mode (II.47 and II.48 equations).

IV.3.2 Comparison between air collector with and without fins: In this part, our objective is to compare the temperature between the air collector with and without fins.

- **Air collector with 49 fins:**

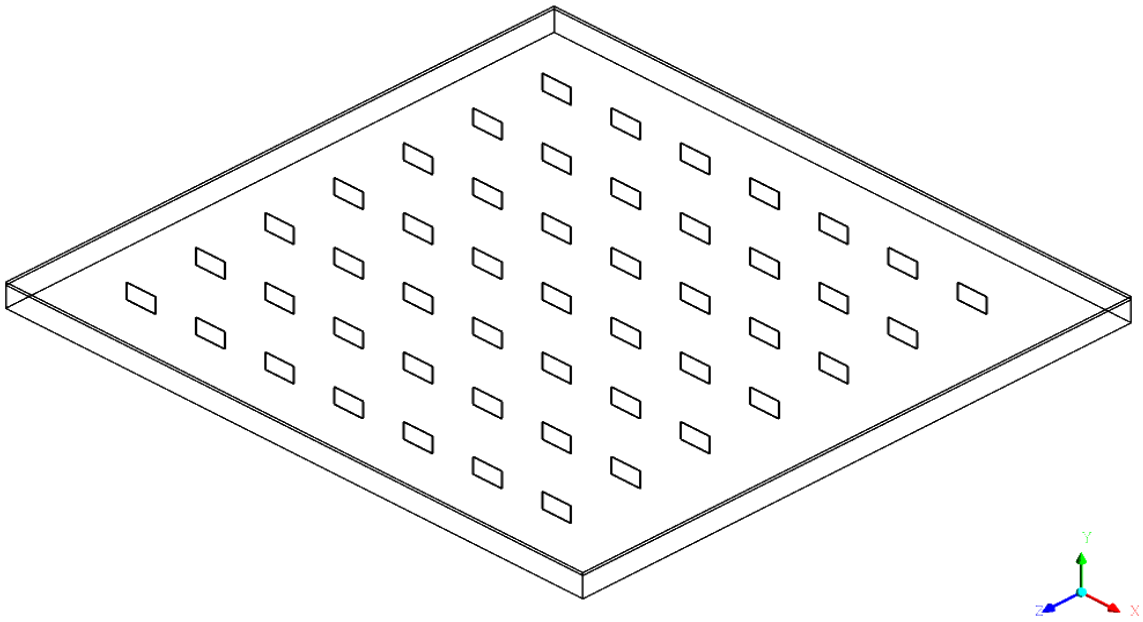

Figure IV.12 Air Collector with Fins

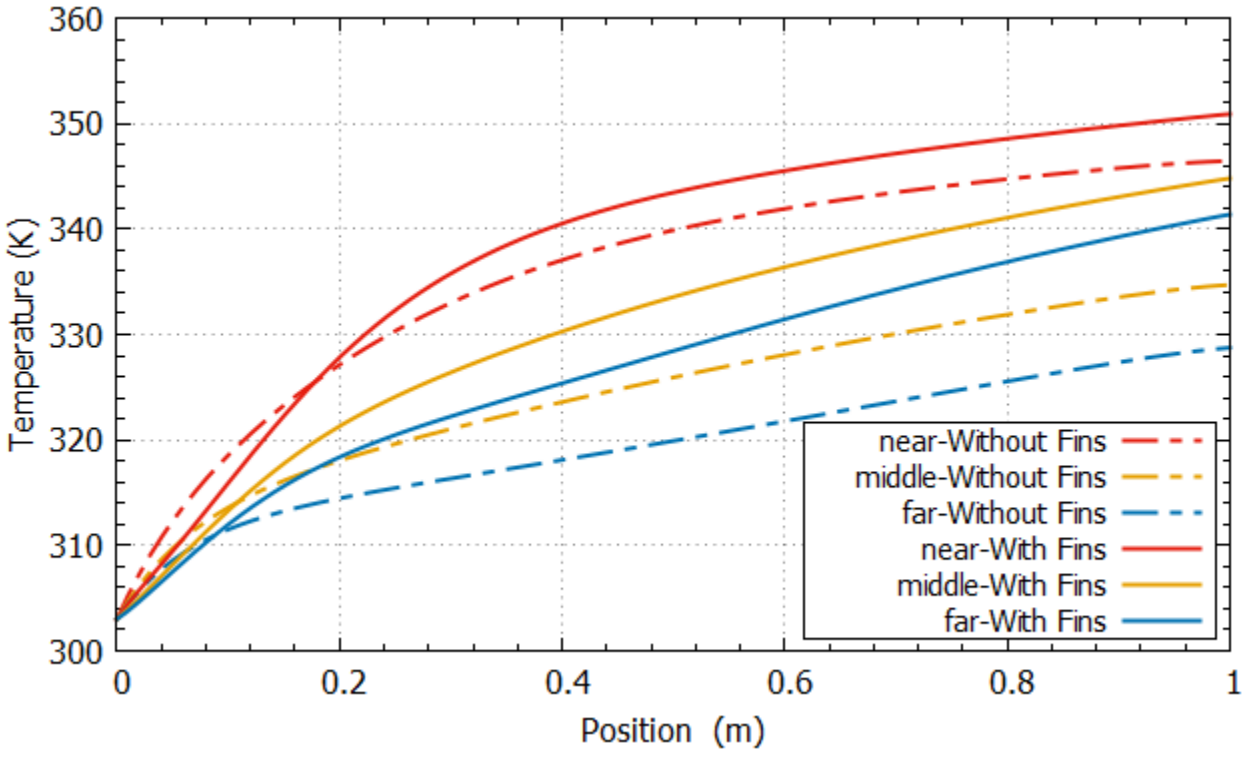

Figure IV.13 Temperature variation between the Air Collector with and without Fins

Figure IV.13, represent the temperature variation of air collector with and without fins at different position, the system with fins is approximately 1.265, 2.927 and 3.701 % higher than without fins for near, middle and far absorber respectively, this indicate that the system with fins receive more the heat than without fins. So the addition of fins to a surface has a significant impact on the efficiency and performance of various objects. by increased surface area allows for more efficient dissipation of heat by providing more contact area with the surrounding air.

Table IV.1 temperature difference between the 3 lines for air collector with and without fins

ΔT / lines	Air velocity 0.05 m/s	
	With fins (49 fin)	Without fins
Near – middle	6.098	11.752
Middle-near insulator	3.427	5.968

This table shows the difference between air homogenization inside a finned and non-finned collector. The collector without fins has a clear double difference compared to the other, in the homogeneity of the air between the top, middle and bottom. This is due to another importance of the fins, which is to increase the homogeneity inside the air, that shown in figure IV.9 and IV.14.

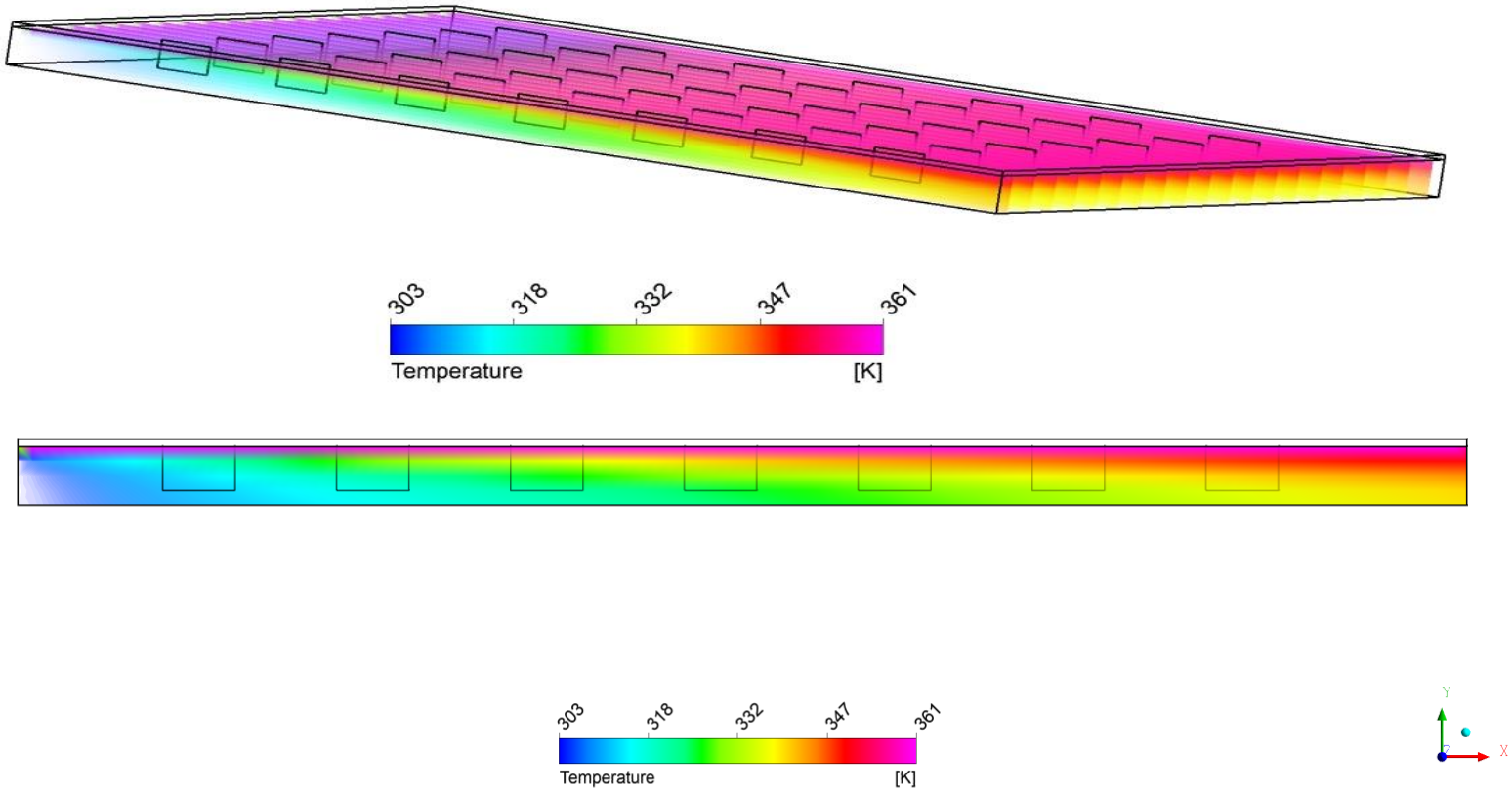

Figure IV.14 Temperature contour of the Air Collector with Fins

IV.3.3 Fin thickness effect: in this part, we simulate it for (0.001,0.003 and 0.005 m) of fin thickness.

- **Air collector with 49 fin, 0.001 m thickness and 0.03 m height:**

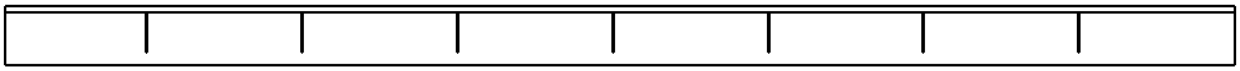

Figure IV.15 Cross section of the Finned Air Collector 0.001 m thickness

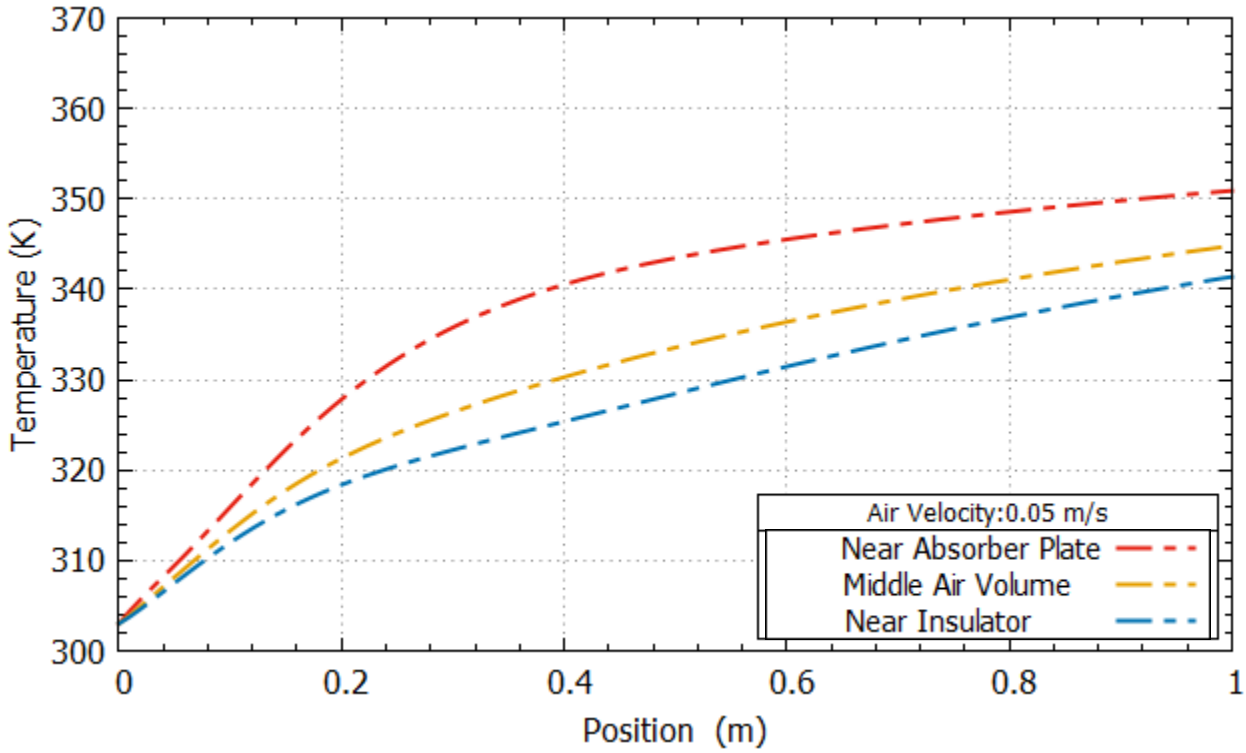

Figure IV.16 The Temperature distribution for the Air Collector with Fins, (0.001m thickness)

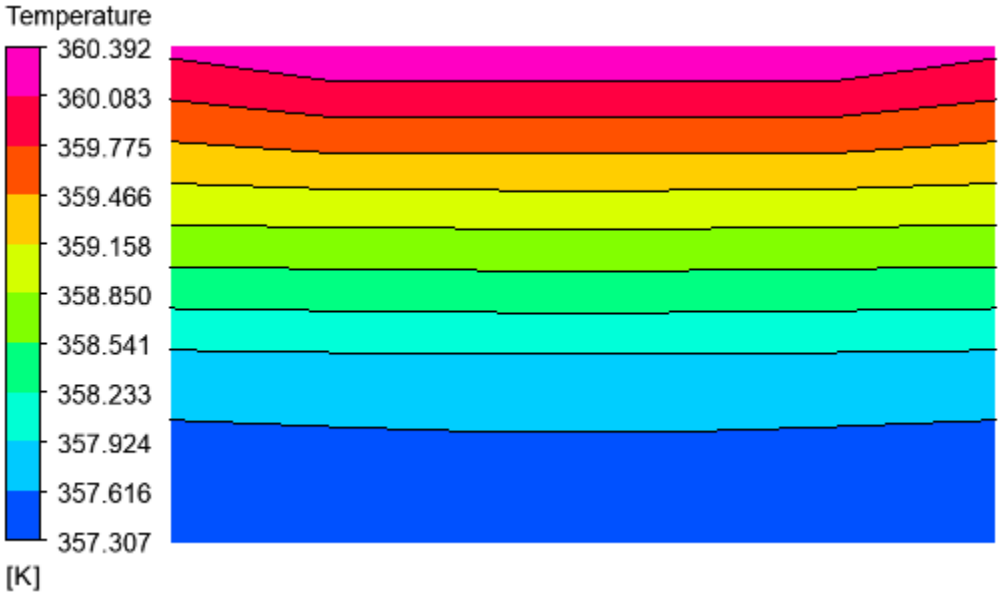

Figure IV.17 Local Temperature distribution for 0.001 fin thickness

- **Air collector with 49 fin, 0.003 m thickness and 0.03 m height:**

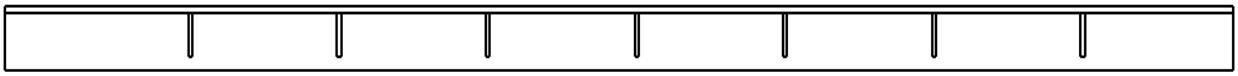

Figure IV.18 Cross section of the Finned Air Collector 0.003 m thickness

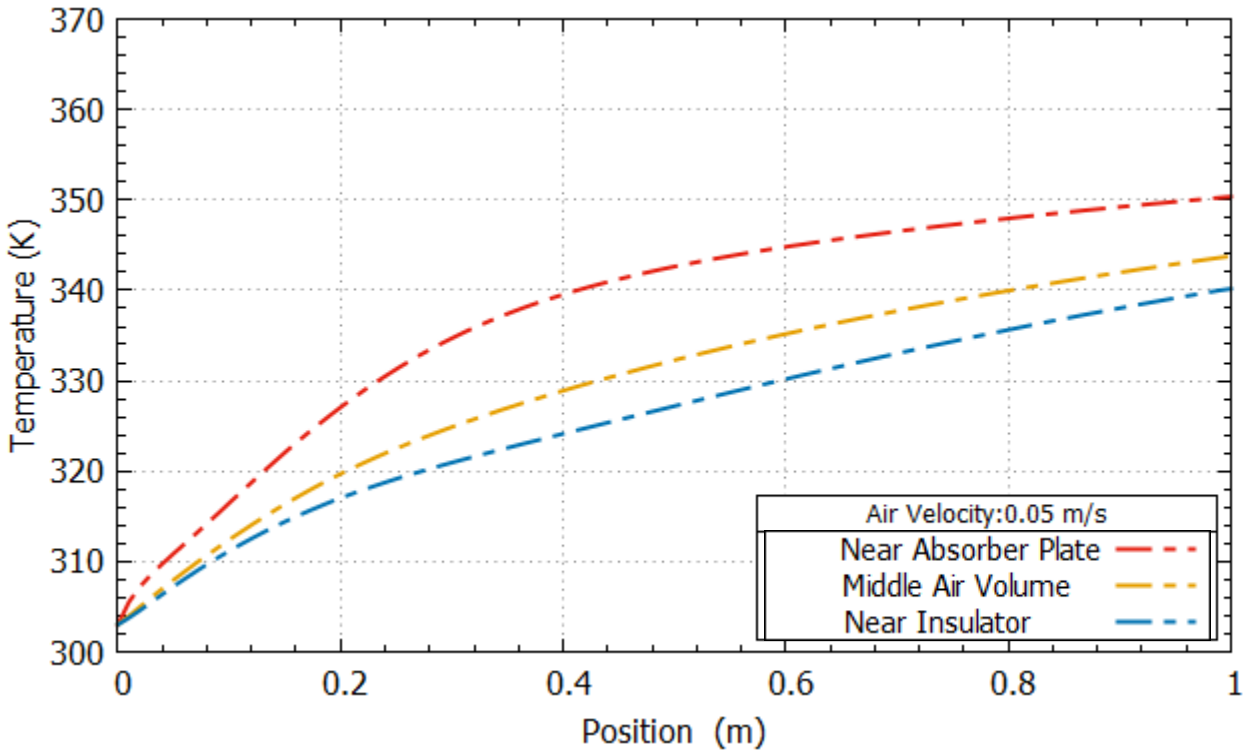

Figure IV.19 The Temperature distribution for the Air Collector with Fins (0.003m thickness)

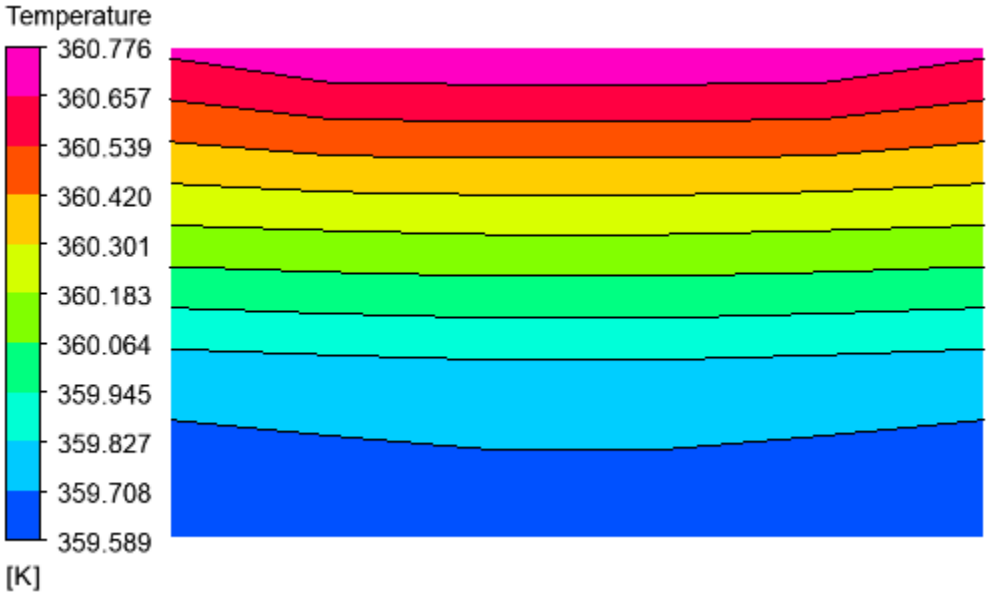

Figure IV.20 Local Temperature distribution for Fin 0.003m thickness

- **Air collector with 49 fin ,0.005 m thickness and 0.03 m height:**

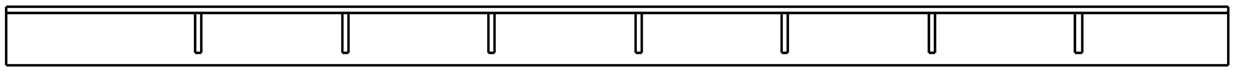

Figure IV.21 Cross section of the Finned Air Collector 0.005 m thickness

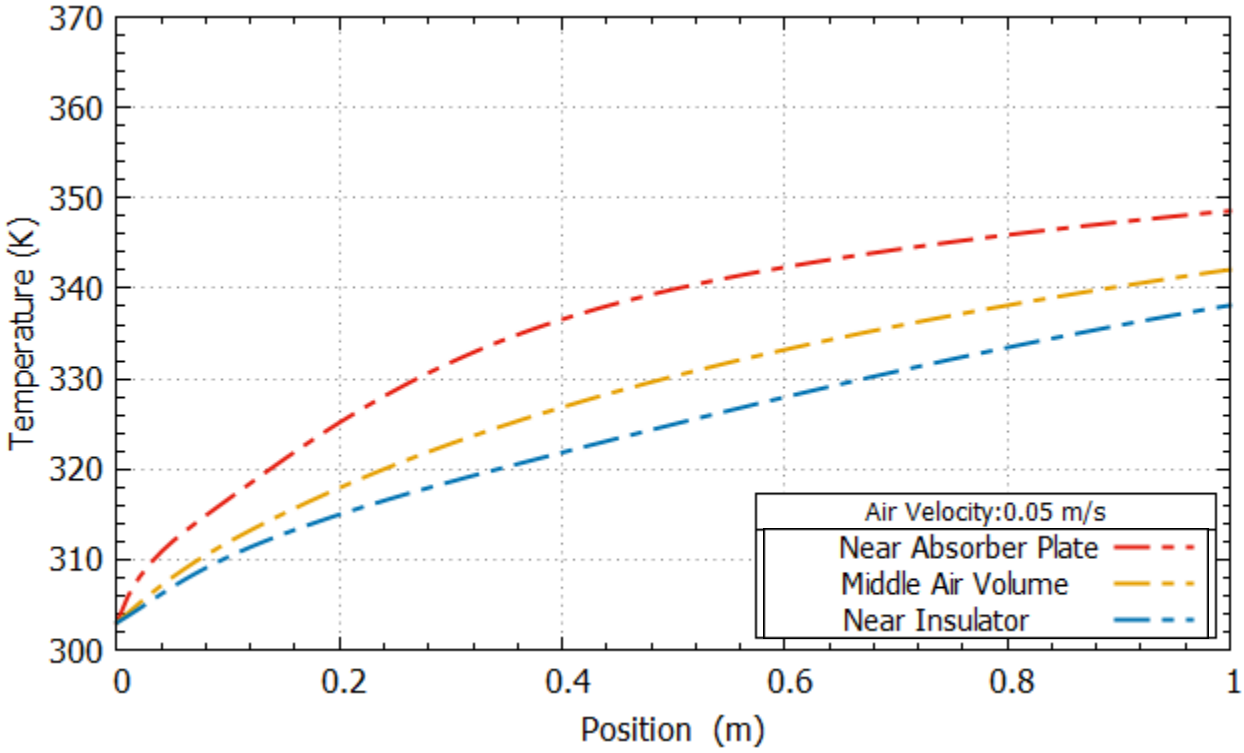

Figure IV.22 The Temperature distribution for the Air Collector with Fins (0.005 m thickness)

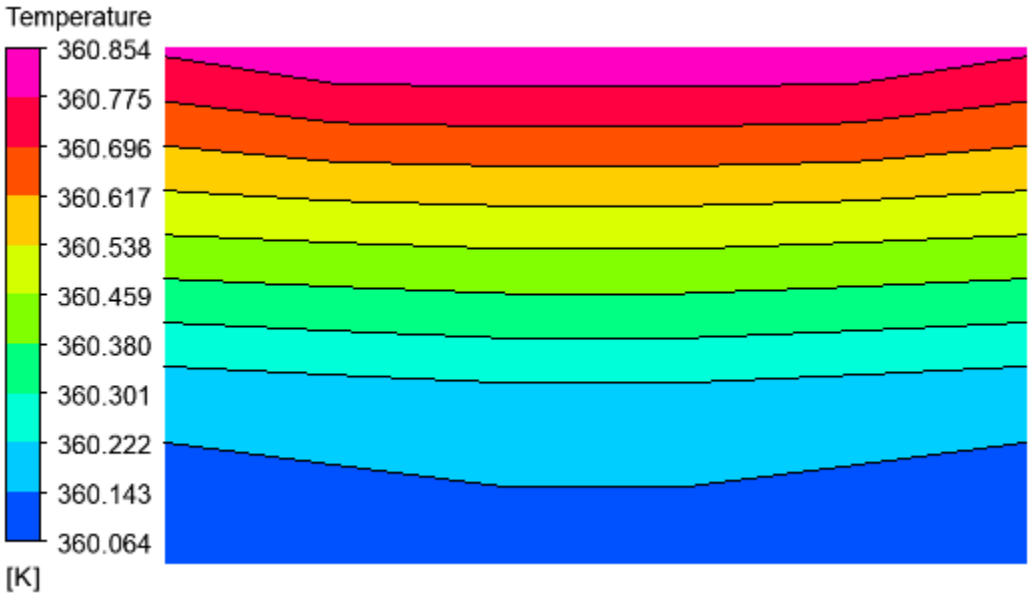

Figure IV.23 Local Temperature distribution for Fin 0.005 thickness

Figure IV.16, IV.19, IV.22, are show the temperature distribution for different thickness (0.001,0.003,0.005) m, at different position. The simulation results have shown that there is an effect of fin thickness, air collector with 0.001 fin thickness is approximately 0.299% And 0.799% higher than with 0.003 and 0.005 fin thickness respectively. Add to that, figure IV.17, IV.20, IV.23, we can see that, there is a different in the fin local temperature, the fin with higher thickness (0.003 and 0.005 m) store more heat, for that the thick fin can't transformed the heat easy. This change explains the difference in the drying temperature of the collector. So the thicker fins tend to have higher conduction resistance, this is because a thicker fin requires heat to travel a greater distance through the material, which can impede the heat transfer process. Conversely the thinner fins offer lower conduction resistance as heat can more easily pass through the shorter distance.

IV.3.4 Fin material effect:

The fin material effect is study for 3 materials (Copper, aluminum and mild steel).

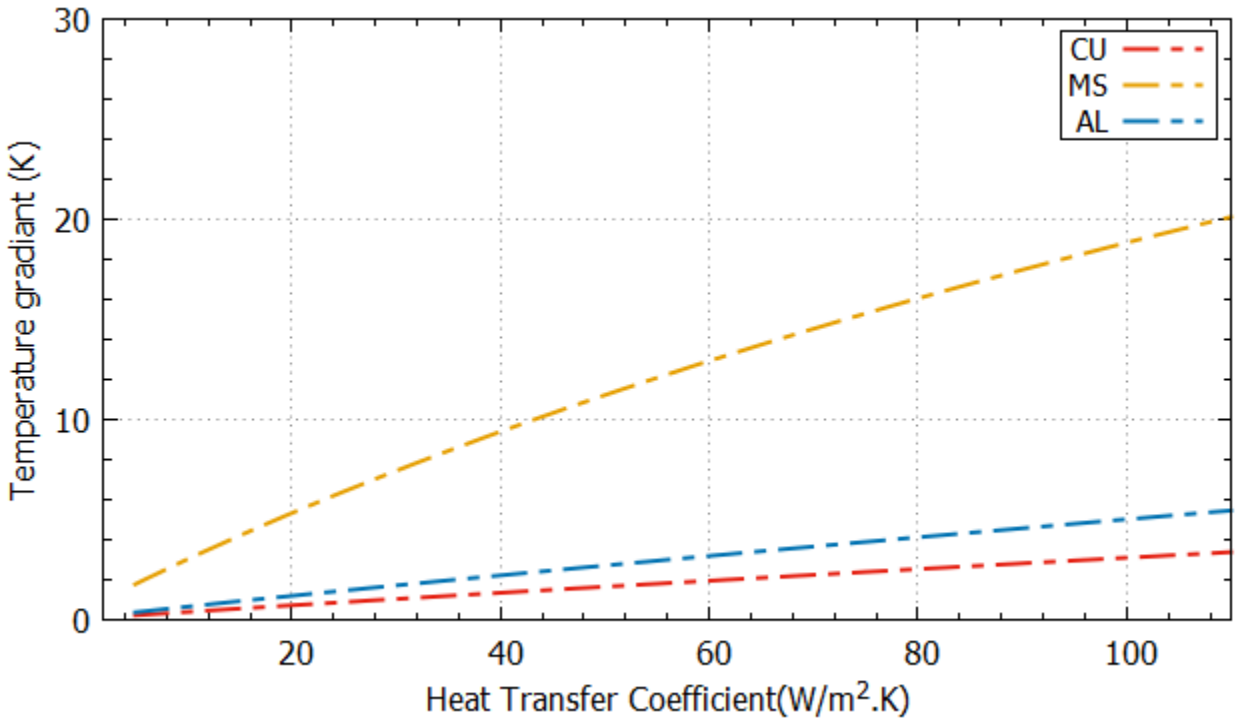

Figure IV.24 Variation of Thermal gradients in Fin

Figure IV.24 compare the fin material of different heat transfer coefficient. As it is evident in figure IV.24 larger thermal gradients exist in M.S. compared to Cu or Al, indicates that M.S. stores more thermal energy rather than transferring it. Hence, the choice of M.S for fin applications is not suggested from heat transfer consideration. On the other hand, the use of Cu for such applications highly recommended as already seen. Further, Aluminum, which has heat transfer performance closer to copper, can also be used as absorber material due to its lower density and cost.

IV.3.5 Fin position effect: in this part, the fin position is treated here

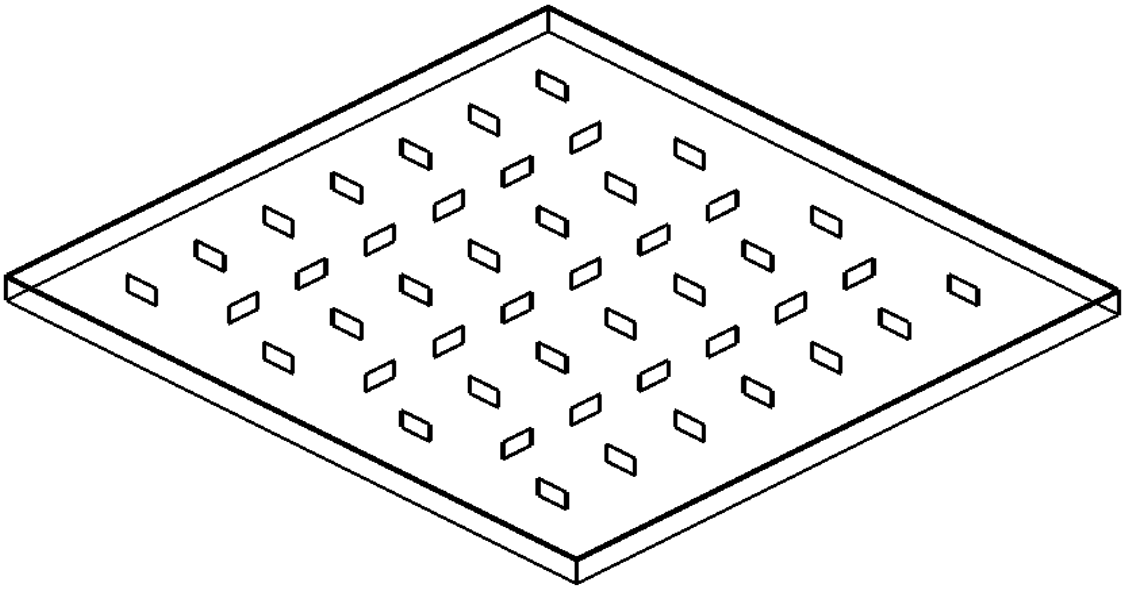

Figure IV.25 Air Collector with Vertical and Horizontal Fins

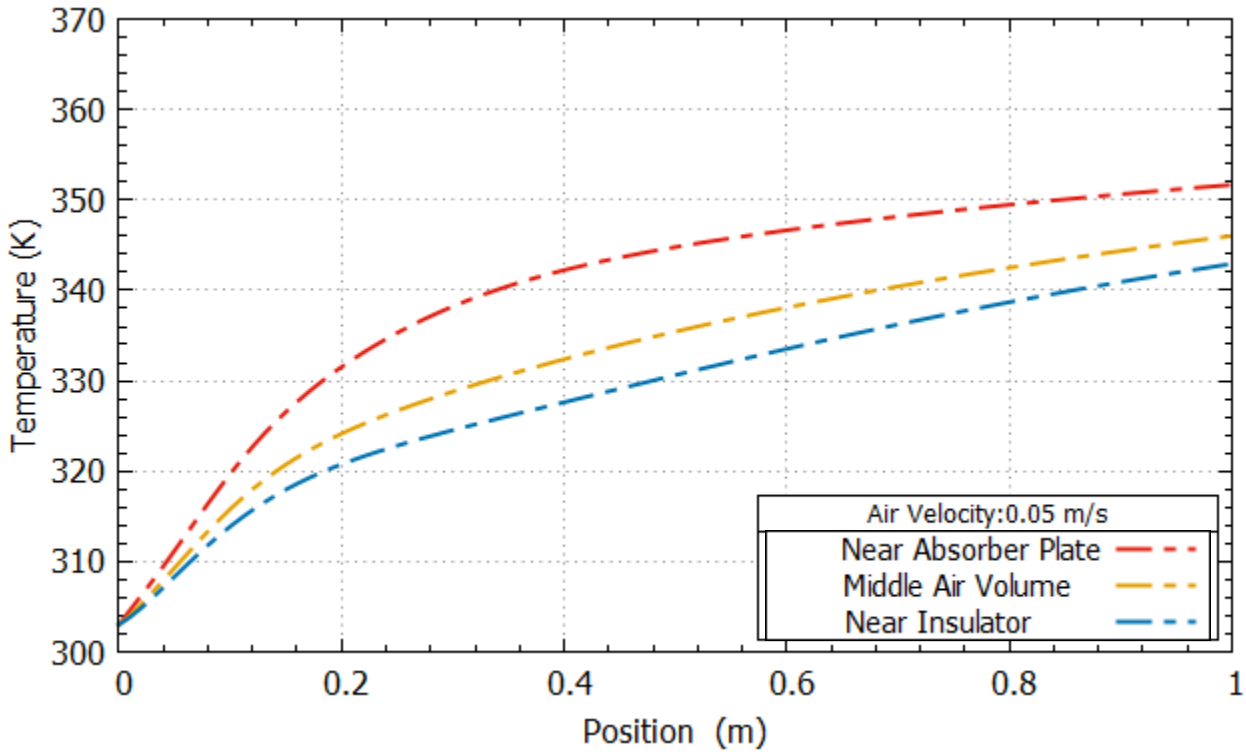

Figure IV.26 The Temperature distribution for the Air Collector with Fins (46 fin,0.001 m thickness and 0.03 m height)

Figure IV.25 show another configuration for fins, its results are explained in figure IV.26. the system with vertical and horizontal fins is approximately 0.350 % higher than with normal fins. So the arrangement and orientation of fins influence the overall fluid dynamics and pressure drop, further impacting system efficiency.

Conclusion:

In conclusion, the Results and Discussion chapter of this dissertation plays a pivotal role in unraveling the results of the research conducted. By presenting the findings and engaging in a thorough analysis. This will contribute to the existing knowledge in the field and guide future research and practical applications.

General Conclusion:

The Algerian experience in solar drying is a recent one, as we cannot find scientific publications dealing with this theme before 1999. The local developed solar dryers are applied essentially to dry different sorts of locally produced foods and medicinal herbs such as dates, tomatoes, figs, apples, grapes, apricots, and mint. [1]

This study allowed us to deepen and consolidate our knowledge about the Fins and the importance of fins characteristics on the air collector in particular and the solar dryer in general.

The characteristics of fins, including their thickness, material, and position, have a significant impact on air collector performance. Through comprehensive research and analysis, this dissertation has shed light on the effects of these parameters on heat transfer, fluid dynamics.

As we found out. After the addition of fins, the system improves by 1.265, 2.927 and 3.701 % than without fins for near, middle and far absorber respectively.

For fin thickness, air collector with 0.001 fin thickness is approximately 0.299% And 0.799% higher than with 0.003 and 0.005 fin thickness respectively. So it has been observed that thinner fins generally offer higher heat transfer rates due to increased surface area. However, there is a limit to how thin a fin can be before it becomes structurally unstable. Therefore, selecting an optimal fin thickness that balances heat transfer enhancement and structural integrity is crucial.

There is an increase in the heat transfer coefficient as air enters and moves along the Collector.

There is a larger thermal gradient in M.S. compared to Cu or Al, indicates that M.S. stores more thermal energy rather than transferring it, Aluminum, which has heat transfer performance closer to copper, can also be used as absorber material due to its lower density and cost. So the choice of fin material also plays a crucial role in determining the effectiveness of heat transfer. Different materials exhibit varying thermal conductivity, corrosion resistance, and cost factors. The selection should consider the specific requirements of the application to achieve optimal performance and durability.

The system with vertical and horizontal fins is approximately 0.350 % higher than with normal fins. So the position of fins within a system also affects heat transfer efficiency. Additionally, the arrangement and orientation of fins can influence the overall fluid dynamics and pressure drop, further impacting system efficiency.

To conclude, this study asserts that fin thickness, fin material and fin position have a direct effect on the performance of finned air collector. Overall, optimizing fin characteristics, is essential for maximizing heat transfer efficiency, system performance, and energy utilization. Future research should continue to explore advanced fin designs and materials to further improve heat transfer capabilities in various fields.

REFERENCES

[1] Lyes Bennamoun, Reviewing the experience of solar drying in Algeria with presentation of the different design aspects of solar dryers, Renewable and Sustainable Energy Reviews 15 (2011) 3371–3379

[2] F.P. Incropera, D.P. Dewitt, Introduction to Heat Transfer, New York: John Wiley &Sons, Inc, 2th edition, 1990.

[3] https://www.greenhousesolardryer.com/2021/05/shall-we-get-to-know-some-facts-regarding-types-of-solar-dryers/#:~:text=Solar%20drying%20technology%20was%20invented,for%20grain%20and%20fish%20drying.

[4] R. Miri, O. Mokrani , F. Siad, M. Belhamel , Etude expérimentale d'un séchoir solaire, Rev. Energ. Ren : Zones Arides(2002) 41-48

[5] Benkhelfellah R, El Mokretar S, Miri R, Belhamel M. Séchoirs solaires. Étude comparative de la cinétique de séchage des produits agroalimentaires dans des modèles de type direct et indirect, 12 èmes Journées Internationales de Thermique 2002:259–62

[6] Benaouda N, Belhamel M. l'expérience du séchage solaire en Algérie. Revue des Énergies Renouvelables 2007 [Special issue: CER'07]

[7] Boulemtafes-Boukadoum A, Benaouda N, Derbal H, Benazaoui A. Analyse énergétique et thermique du processus de séchage de la menthe par énergie solaire. Revue des Énergies Renouvelables 2008:89–96 [Special issue: SMSTS'08]

[8] Messaoud Sandali, Abdelghani Boubekri, Djamel Mennouche , Numerical study of the Thermal Performance of a Direct Solar Dryer with Integrated Geothermal Water Heat Exchanger, Manuscript ID_310

[9] Messaoud Sandali , Abdelghani Boubekri , Djamel Mennouche ,Noureddine Gherraf , Improvement of a direct solar dryer performance using a geothermal water heat exchanger as supplementary energetic supply. An experimental investigation and simulation study, Renewable Energy 135 (2019) 186e196

[10] B.M.A. Amer , M.A. Hossain , K. Gottschalk , Design and performance evaluation of a new hybrid solar dryer for banana, Energy Conversion and Management 51 (2010) 813–820

[11] S. Nabnean , S. Janjai , S. Thepa , K. Sudaprasert , R. Songprakorp , B.K. Bala , Experimental performance of a new design of solar dryer for drying osmotically dehydrated cherry tomatoes, Renewable Energy 94 (2016) 147e156

[12] M. Yahya , Ahmad Fudholi , Kamaruzzaman Sopian , Energy and exergy analyses of solar-assisted fluidized bed drying integrated with biomass furnace, Renewable Energy 105 (2017) 22e29

[13] T Bhattacharyya, R Anandalakshmib, K. Srinivasan ,Heat Transfer Analysis on Finned Plate Air Heating Solar Collector for its Application in Paddy Drying, Energy Procedia 109 (2017) 353 – 360

[14] Panuwat Pawakote, and Atit Koonsrisuk, Design of a solar dryer with fins and baffles for rice-cracker drying, Materials Science and Engineering 383 (2018) 012065

[15] C. UMA MAHESWARI1, R. MEENAKSHI REDDY & BURIGALA VINODH, DESIGN AND CFD ANALYSIS OF FOOD DRYER USING SOLAR FLAT PLATE COLLECTOR AND EXHAUST GAS WITH FINNED COPPER TUBES, IJMPERDDEC201838

[16] Satyapal Yadav, V.P. Chandramohan, Performance comparison of thermal energy storage system for indirect solar dryer with and without finned copper tube, Sustainable Energy Technologies and Assessments 37 (2020) 100609

[17] S. Murali*, P.R. Amulya, P.V. Alfiya, D.S. Aniesrani Delfiya, Manoj P. Samuel , Design and performance evaluation of solar - LPG hybrid dryer for drying of shrimps, Renewable Energy 147 (2020) 2417e2428

[18] Cristiana Brasil Maia, Gisele Mol da Silva, Luiz Felippe Guardia Bianchi and André Guimarães Ferreira, Performance study of a baffled solar dryer, 10.3934/energy.2021052

[19] Erdem Çiftçi , Ataollah Khanlari , Adnan Sozen , Ipek Aytaç , Azim Dogus¸ Tuncer, Energy and exergy analysis of a photovoltaic thermal (PVT) system used in solar dryer: A numerical and experimental investigation, Renewable Energy 180 (2021) 410e423

[20] S. Madhankumar , Karthickeyan Viswanathan , Wei Wu , Muhammad Ikhsan Taipabu , Analysis of indirect solar dryer with PCM energy storage material: Energy, economic, drying and optimization, Solar Energy 249 (2023) 667–683

[21] Ikem Azorshubel Ikem, M. I. Ibeh, Ukwenya John , Estimating The Efficiency Of Okra Drying Mixed-Mode Solar Dryer, Article in International Journal of Engineering Research · January 2017.

[22] T Bhattacharyya, R Anandalakshmib, K. Srinivasan ,Heat Transfer Analysis on Finned Plate Air Heating Solar Collector for its Application in Paddy Drying, Energy Procedia 109 (2017) 353 – 360.

[23] Wattmuff, J.H., Charters, W.W.S., Proctor, D., 1977. Solar and wind induced external coefficients for solar collectors. Internationale Revue d'Heliotechnique 2, 56.

[24] Frank P.Incropera, David P. DeWitt,Fundamentals of Heat and Mass Transfer ,-3rd ed .

[25] Warren M. Rohsenow , James R Hartnett, Young I. Cho , Handbook of heat transfer, Third Edition.

[26] Braham Chaouch Wafa, Etude de la cinétique de séchage de la viande cameline par séchoir de la region d'adrar , (Doctoral dissertation), University of SAAD DAHLEB, Blida

[27] G Satyanarayana, K. pavan kumar, G. Veeraiah, M Y Prasada Ra, Ch Varun, SS Naidu, GEOMETRICAL OPTIMIZATION OF FINS FOR EFFECTIVE HEAT TRANSFER USING CFD ANALYSIS, International Research Journal of Engineering and Technology (IRJET) Volume: 06 Issue: 11 | Nov 2019

[28] fluent guide